8 Lateral superlattices

8.1 Geometrical quantization

For an introduction into the phenomenon of geometrical quantization see Section 7.1 on page 116.

8.1.1 Magnetic depopulation

For an introduction into the phenomenon of magnetic depopulation see Section 7.1.1 on page 116.

Brinkop et al [88B1] (page 244) measured MR in an array of parallel GaAs wires. For $B > 0.5$ T, quantum oscillations became visible in dR/dV_g as a function of B. A fan diagram showed a deviation from a linear 2D behaviour at low magnetic fields, reflecting quantization of the electronic motion by the lateral confining potential.

Alsmeier et al [88A] (page 244) measured MR of multi–wire inversion channels on InSb. In dR/dV_g vs. B, oscillations due to 1D subband quantization (subband spacing $\approx$ 10 meV) were observed.

Demel et al [88D] fabricated shallow etched (A) and deep etched (B) GaAs single–layer quantum wire arrays and a deep etched (C) GaAs double–layer quantum wire array ($a = 500 - 1100$ nm, $w \approx 250 - 550$ nm) by holographic lithography and RIE. Magneto transport measurements revealed SdH oscillations with a period non–linear in $1/B$ in sample A (Fig. 217), reflecting the 1D character of the structure (subband spacing 2.3 meV, six subbands occupied). In the quasi–dc conductivity of sample B (measured by microwave transmission), SdH oscillations also showed a deviation from a linear $1/B$ behaviour (Fig. 218, subband spacing 1.0 meV, 12 subbands occupied). Finally, the quasi–dc magneto transport of sample C showed SdH oscillations (Fig. 219) which did not follow $1/B$ (subband spacing 1.5 meV, 16 subbands occupied). In [89D2] Demel et al performed again MR measurements on single and multi–layered wire arrays and found typical subband separations of 1 to 3 meV in electron channels of 150 to 400 nm width.

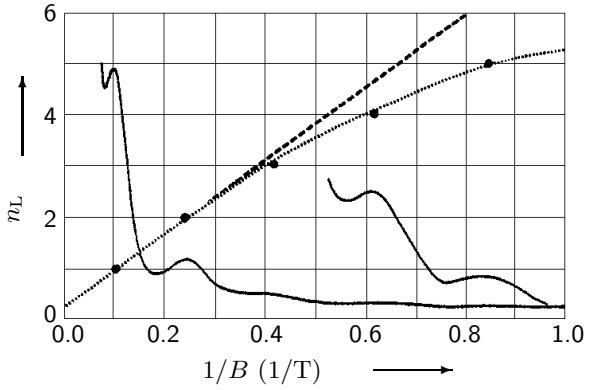

Fig. 217: MR measurements (full lines, no scale) on sample A plotted vs. $1/B$ [88D]. A fan chart for the positions of the maxima in the MR (full circles, left scale) exhibited deviations from a linear $1/B$ dependence (dashed line). The dotte line shows the depopulation of 1D subbands within a harmonic oscillator model.

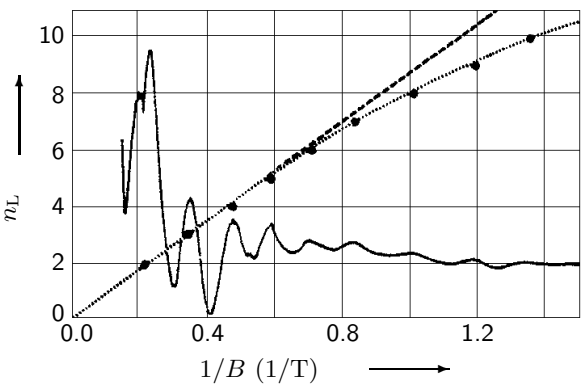

Fig. 218: MR measurements (full lines, no scale) on sample B plotted vs. $1/B$ [88D]. A fan chart for the positions of the maxima in the MR (full circles, left scale) exhibited deviations from a linear $1/B$ dependence (dashed line). The dotte line shows the depopulation of 1D subbands within a harmonic oscillator model.

Merkt [89M5] performed MR measurements on parallel InSb and GaAs wires. He observed SdH oscillations, Landau plots deviated from a straight line. Subband spacings were estimated.

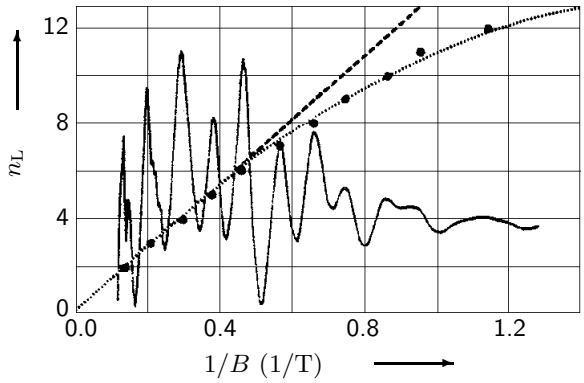

Fig. 219: MR measurements (full lines, no scale) on sample C plotted vs. $1/B$ [88D]. A fan chart for the positions of the maxima in the MR (full circles, left scale) exhibited deviations from a linear $1/B$ dependence (dashed line). The dotted line shows the depopulation of 1D subbands within a harmonic oscillator model.

Kern et al [90K3] fabricated wire arrays on InGaAs by holographic lithography and RIE ($a = 575\,\text{nm}$, $w = 150 - 450\,\text{nm}$). In quasi–dc magneto transport experiments at 2.2 K (performed by measuring the transmission of microwaves), SdH oscillations were observed. The index of the oscillations did not depend linearly on $1/B$ at small B, demonstrating a 1D confined energy spectrum (subband spacing 2.5 meV, 15 subbands occupied in a 300 nm wide wire).

Gao et al [90G3] (page 226) examined 1D subband effects in 240 parallel Si wires. The dependence of $\partial G/\partial V_g$ on magnetic field (for fields up to 20 T) showed oscillations attributed to the SdH effect. The positions of the maxima vs. $1/B$ deviated from a linear behaviour at small B.

Hirler et al [90H] presented measurements of 1D subband energies in arrays of GaAs wires having different geometrical widths ($a = 1000$, 450, and 300 nm) fabricated by wet etching. An overall gate covered the sample. The differential MR, dR/dV_g, was measured as a function of magnetic field and gate voltage. A Landau plot of the MR oscillations showed deviations from a linear behaviour in $1/B$, indicating the existence of 1D subbands. The deviation from linearity increased with decreasing V_g and decreasing grating period. The dependence of the channel width, the subband spacing, and the 1D electron concentration on gate voltage was examined. In addition, tunneling experiments were performed with and without magnetic field in order to measure the 1D subband energies directly. The subband spacing increased in a magnetic field

Demel et al [91D] performed magneto transport measurements on parallel GaAs wires ($w = 150 - 400\,\text{nm}$) fabricated by holographic lithography and deep etching. The MR (at $T = 2.2\,\text{K}$) exhibited SdH oscillations. Landau plots deviated from a linear behaviour indicating the formation of 1D subbands. The electron density could be increased by illuminating the wires with short pulses from a red LED. With increasing electron density, the subband separation decreased.

Mani et al [92M2, 94M5] (page 244) investigated arrays of parallel GaAs wires. The two–terminal MR exhibited SdH oscillations (Fig. 241). The extrema positions as a function of $1/B$ deviated from a linear behaviour (confinement energy $0.5 - 1.0\,\text{meV}$, $7 - 11$ subbands occupied).

Berthold et al [93B4] (page 237) performed magneto transport experiments in arrays of parallel GaAs wires. MR measurements at $T = 3\,\text{K}$ revealed SdH oscillations above $B = 1\,\text{T}$. A Landau plot showed deviations from a linear behaviour and subband spacings of 2.5 meV and 1.0 meV were estimated. Subband spacings determined from magnetophonon resonances were 7.2 meV and 2.6 meV.

Motohisa et al [93M4] (page 245) fabricated 100 parallel GaAs wires by cleaved edge overgrowth, measured the MR at different angles and observed SdH oscillations. A Landau plot showed deviation from a straight line, demonstrating the quasi 1D nature of the electronic states (subband spacing $\approx 2.2\,\text{meV}$, five subbands occupied at $B = 0\,\text{T}$.)

Holzmann et al [95H4, 96H3] (page 238) fabricated arrays of ≈ 300 Si wires in parallel and measured the two–terminal MR at $T = 360 \pm 10\,\text{mK}$. Landau plots showed deviations from linear

behaviour, demonstrating the existence of 1D subbands (Fig. 236). A subband spacing of $\hbar\omega_0 = 0.3 - 1.0\,\mathrm{meV}$ was extracted. In the smallest wire, only four subbands were occupied.

Hauser et al [94H3] (page 238) investigated transport in arrays of parallel GaAs wires. SdH oscillations were observed, Landau plots deviated from a linear $1/B$ dependence. The height of the confinement potential was obtained from the Landau plots.

Ploner et al [96P1, 97P, 98P2] (page 240) performed magnetophonon resonance studies on arrays of forty parallel quantum wires. From the MPR, subband spacings of $1.6 \pm 0.3\,\mathrm{meV}$ were deduced, while those inferred from magnetic depopulation experiments were $1.1 \pm 0.3\,\mathrm{meV}$. They explained the difference between the subband spacings via the deviation of the actual confinement potential from a parabolic shape. The theoretical fits yielding the subband spacings were based on a parabolic confinement.

Sasa et al [96S1] fabricated arrays of ten parallel wires of InAs/AlGaSb ((A) $w = 0.2\,\mu\mathrm{m}$, $L = 10\,\mu\mathrm{m}$; (B) $w = 0.3\,\mu\mathrm{m}$, $L = 10\,\mu\mathrm{m}$; (C) $w = 0.4\,\mu\mathrm{m}$, $L = 10\,\mu\mathrm{m}$) by photolithography and wet chemical etching. They performed MR measurements for $0\,\mathrm{T} < B < 8\,\mathrm{T}$ at 4.2 K and observed SdH oscillations. Landau plots showed deviations from a linear behaviour for all samples. Sasa et al estimated the 1D electron concentration, the effective wire width and the subband spacing. Further, they measured I–V characteristics and studied the mobility as a function of electric field.

Lefebvre et al [98L] fabricated an array of GaAs wires (period 400 nm) defined by split gates ($w = 200\,\mathrm{nm}$, $L = 200\,\mu\mathrm{m}$). The electrical resistance at $T = 1.9\,\mathrm{K}$ and $B = 0\,\mathrm{T}$ was measured for a current parallel and perpendicular to the stripes for different gate voltages. A weak modulation was already present at zero gate voltage. Below $-0.43\,\mathrm{V}$, electrical conduction became impossible in the perpendicular configuration. MR measurements showed magnetic depopulation. For a gate voltage of $-0.8\,\mathrm{V}$, a subband spacing of 1.2 meV was found. Lefebvre et al performed also optical measurements on the sample.

8.1.2 Quantized conductance

For an introduction into the phenomenon of quantized conductance see Section 7.1.2 on page 118.

Warren et al [86W4] fabricated Si devices in which a periodic gate ($a = 0.2\,\mu\mathrm{m}$) was used to define 250 narrow ($w \approx 50\,\mathrm{nm}$, $L = 10\,\mu\mathrm{m}$) inversion lines in parallel. The electron density could be varied by the help of a second gate. Warren et al measured current vs. upper gate voltage (controlling the Fermi energy) and found a weak modulation at 1.2 K (Figs. 220 and 221). Differentiation revealed a regular weak oscillation of conductance with gate voltage (period $1 - 1.5\,\mathrm{V}$). The modulation could also be observed at 4.2 K and very weakly at temperatures approaching 10 K. Warren et al assumed to have observed a 1D density of states in the modulation of conductance with gate voltage.

Ismail et al [89I] reported on transport measurements on 100 parallel GaAs wires ($w_{\mathrm{eff}} = 35\,\mathrm{nm}$, $L = 5$ and $10\,\mu\mathrm{m}$, $l = 1\,\mu\mathrm{m}$). The source–drain current as a function of substrate bias (controlling the Fermi energy) exhibited structure at 4.2 K (and even at 77 K) which was attributed to the presence of 1D subbands (subband spacing 1 meV). A conductance perpendicular to the wires became measurable for a substrate bias around 6.8 V and was about 500 times smaller than the parallel wire conductance.

Gao et al [90G3] examined 1D subband effects in 240 parallel Si wires ($a = 200\,\mathrm{nm}$, $w = 60 - 80\,\mathrm{nm}$) defined by a negative voltage on a lower gate. A positive voltage on an upper gate created inversion. The conductance as a function of upper gate voltage did not show UCF (indicating an effective averaging). The derivative $\partial G/\partial V_{\mathrm{g}}$ oscillated regularly, reflecting the quasi–1D density of states. The subband spacing was $\approx 1.2\,\mathrm{meV}$, the number of occupied subbands as a function of upper gate voltage was investigated. The dependence of $\partial G/\partial V_{\mathrm{g}}$ on magnetic field (for fields up

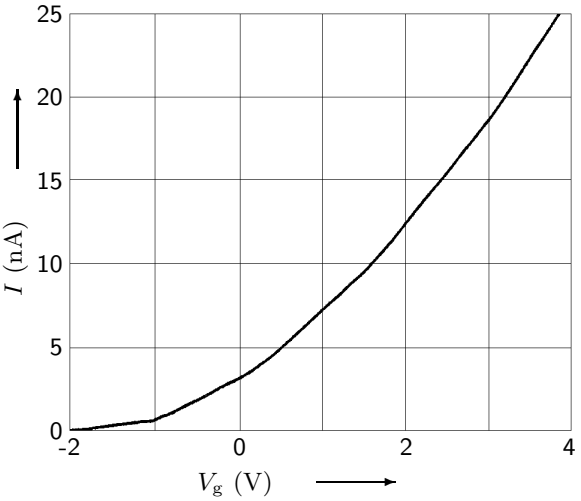

Fig. 220: Source drain current vs. upper gate voltage at $T = 1.2\,\mathrm{K}$ and a voltage of $0.5\,\mathrm{V}$ on the periodic gate [86W4].

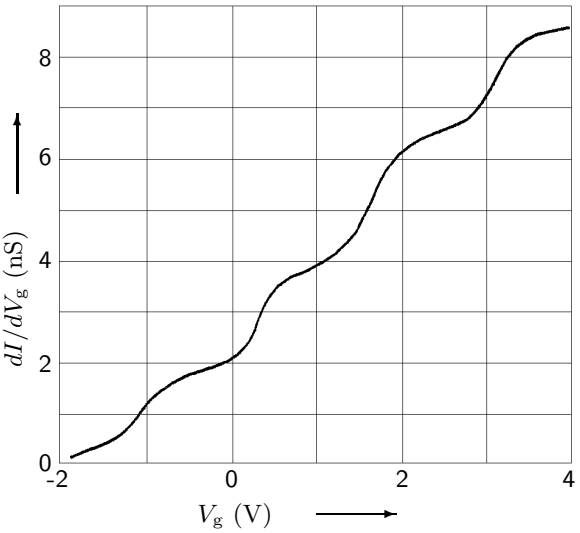

Fig. 221: Derivative of source drain current with respect to upper gate voltage vs. upper gate voltage at $T = 1.2\,\mathrm{K}$ [86W4].

to 20 T) showed oscillations attributed to the SdH effect. The positions of the maxima vs. $1/B$ deviated from a linear behaviour at small B.

Nakata et al [91N] (see page 147) fabricated single GaAs wires using Ga FIB implantation and multiple wire structures by raster scanning a Ga-FIB with periods ranging from $0.24\,\mu$m to $0.60\,\mu$m. They measured current vs. gate voltage in the wire arrays and observed an indistinct structure corresponding to peaks in the conductance vs. V_g. Nakata et al discussed geometrical quantization as a possible origin and extracted a subband spacing of 2.2 meV.

Ismail et al [91I2, 91L1] (see page 270) reported AB oscillations in arrays of GaAs rings. Further, the conductance of the rings showed a step–like behaviour as a function of gate voltage at 4.2 K. Similar steps were observed in $2-4\,\mu$m long single wires as well as in ten parallel wires. The step heights in the single wires were $2 \cdot e^2/h$ and $20 \cdot e^2/h$ in the parallel wires.

Bagwell et al [92B4] (page 241) studied a dual gate Si MOSFET with a grating gate (bottom) and a continuous gate (top). They performed various measurements of G vs. top–gate voltage for different bottom–gate voltages, different magnetic fields, and different temperatures. At very large magnetic fields, $B > 20\,\mathrm{T}$, quantized two-terminal conductance emerged.

Friedland et al [99F2] realized an array of a few quantum wires utilizing multiatomic step arrays (lateral periodicity of 250 nm) at the interface of GaAs/AlGaAs heterostructues. The 2D electron transport was highly anisotropic. Metallic gates constricted the array to a width of $300-500\,$nm. The length of the constriction was $1-2\,\mu$m. The conductance parrallel to the array showed distinct steps up to 10 K. They were attributed to 1D conductance of several parallel conducting wires. SdH oscillation measurements revealed independent conductance along the parallel wires and 1D confinement. The lateral position of the effective width inside the constriction could be varied by independent side–gate control. Single quantum wires could be selected.

8.2 Finite temperature

8.2.1 Conductance in general

For an introduction into the behaviour of the conductance as a function of temperature see Section 7.3.1 on page 132.

Skocpol et al [82S1, 83S] fabricated Si MOSFETs with channel widths of 100 nm ($L = 5\,\mu$m). The wires formed by an array of fourteen parallel narrow gates were compared with a 2D system. The four–terminal conductance was measured as a function of gate voltage and temperature. The conductance G vs. V_g for a narrow and a wide device is shown in Fig. 222. The narrow channels exhibited a strong variation of conductance with temperature due to a combination of weak localization and interaction effects. Fig. 223 shows the temperature dependence of G at fixed $V_g - V_{th}$ (V_{th} threshold voltage) for the same devices as in Fig. 222 after annealing, which unloaded charged traps and decreased the threshold voltage.

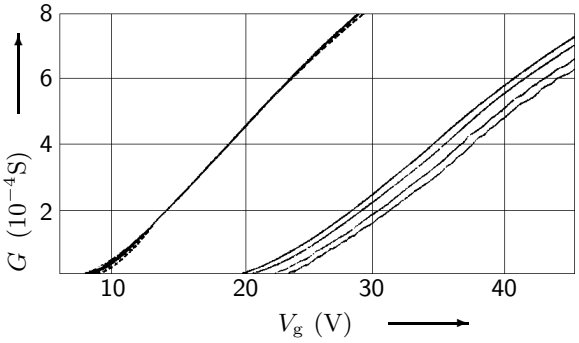

Fig. 222: Conductance G vs. V_g for the wide (left) and the narrow (right) device at (top) $T = 20$ K, 10 K, 4.2 K, and 2.3 K (bottom) [82S1].

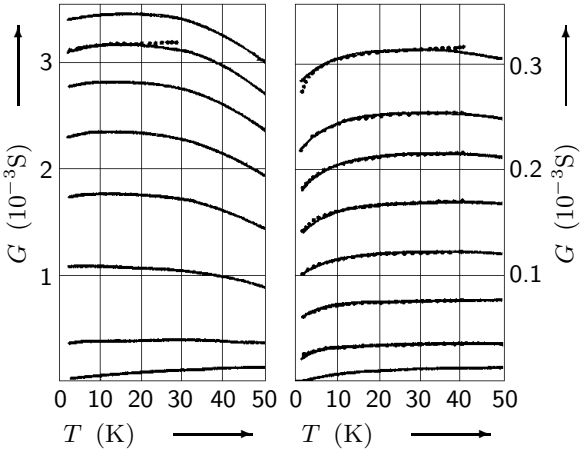

Fig. 223: Conductance vs. temperature for the wide (left) and the narrow (right) device of Fig. 222 after an overnight anneal at 333 K. Curves were taken at (top) $V_g - V_{th} = 40$, 30, 25, 20, 15, 10, 5, and 2 V (bottom). Dotted curves are theoretical fits.

Potts et al [90P2] (page 241) measured conductance vs. temperature in (A) thirty parallel free–standing GaAs wires and in (B) thirty parallel supported GaAs wires. The conductance per unit length per wire of sample A varied as $\ln(T)$ over the range $0.47\,\text{K} < T < 10.0\,\text{K}$ due to a combination of 1D weak localization and 3D interaction effects (Fig. 238).

Hasko et al [93H2] reported fabrication of eight parallel free–standing GaAs wires ($w = 0.5\,\mu$m, $L = 20\,\mu$m) defined by wet etching (down to the semi–insulating substrate) and overgrowth and found that the resistance depended strongly on temperature, characteristic of hopping conduction. Below 1 K, a transition from 3D to 1D hopping was observed.

Gershenson et al [97G2] (page 247) studied the temperature dependence of resistance in five parallel 40 μm long GaAs wires. It was consistent with the theory of quantum corrections due to weak localization and electron–electron interaction effects at high enough T. At low T, the dependence of R on T became exponential and was fitted with an activation law (Fig. 243). Below $T \approx 0.1$ K, the increase of $R(T)$ saturated.

Tang et al [98T3] used an optical method to study carrier diffusion in quantum wire arrays structured on $(InP)_2/(GaP)_2$. The diffusion length along the wire increased with increasing temperature.

Khavin et al [98K5] (page 247) studied the resistance of arrays of GaAs wires. At high temperatures, the resistance increased slowly with decreasing T in accordance with WL theory, while it showed an activation–type behaviour at low T. On the SL side of the crossover the resistance was fitted by $R(T) = R_0 e^{T_0/T}$. The non–linear I–V characteristics was measured at different temperatures. For $V < 5\,\mathrm{mV}$, R was strongly temperature dependent, corresponding to the SL regime. In the WL regime for $V > 5\,\mathrm{mV}$, all $R(V,T)$ fell onto a single curve. Khavin et al estimated the distance between the critical hops L_c from fits of $R(V,T)$ in the SL regime. With decreasing T, L_c increased. The temperature dependence of L_c contradicted predictions based on the VRH theory.

8.2.2 Magneto resistance

This Section contains descriptions of experiments in which the temperature dependence of different phenomena observed in the MR was examined.

Pohlmann et al [86P1] (page 236) fabricated an array of narrow parallel Si inversion channels and measured current vs. gate voltage at different magnetic fields. At high B, giant oscillations were observed in the MC (Fig. 230), the conductance maxima increased with decreasing temperature.

Potts et al [90P2] (page 241) performed four–terminal magneto transport experiments at 15 different temperatures in magnetic fields up to 0.15 T on (A) thirty parallel free–standing GaAs wires and on (B) thirty parallel supported GaAs wires. The data was fitted by 1D weak–localization theory.

Mani et al [92M2, 94M5] (page 244) fabricated arrays of parallel GaAs wires and observed SdH oscillations in the two–terminal MR (Fig. 241). The amplitude of the SdH oscillations showed a stronger temperature dependence with increasing B. In the four–terminal resistance, the SdH linewidth narrowed on the high–field side of the oscillations with decreasing temperature and remained relatively unaffected by T on the low–field side. Mani et al examined the half width at half maximum on the high–field side of the SdH peak, ΔB, as a function of temperature and found $\Delta B \propto T^{0.4(\pm 3\%)}$. They interpreted their results in terms of temperature–induced electronic localization.

Mani et al [93M3, 94M5] (page 237) performed MR measurements on arrays of GaAs wires. A resistance peak at $B = 0\,\mathrm{T}$ increased with decreasing T. At $B = 300\,\mathrm{mT}$, the resistance of a $77\,\mu\mathrm{m}$ long wire increased by a factor of 3.4 upon reducing T from 1.2 to 0.05 K, while the resistance of a $98\,\mu\mathrm{m}$ long wire changed by a factor of 1.6 (Figs. 232 and 233). The results were analysed using temperature power laws which were characteristic of electron–electron interaction and quantum interference effects.

Mani et al [95M2] (page 245) investigated the two–terminal MR of ≈ 300 parallel GaAs wires (Fig. 242). The SdH minima saturated to a temperature–independent behaviour in the vicinity of $\nu = 1$ and $\nu = 2$ at low T. At larger temperatures, $1.5\,\mathrm{K} \leq T \leq 5\,\mathrm{K}$, a $\nu = 1$ resistance minimum in a 810 nm period sample revealed localization and activated transport.

Reulet et al [95R1] (page 243) examined weak localization in ten parallel, quasi–ballistic GaAs wires. The negative MR peak became sharper with decreasing temperature. AF were observed whose amplitude increased with decreasing T

Katine et al [98K3] (page 243) performed MR measurements on an array of GaAs wires defined by a split gate. Weak localization was observed, lower temperatures resulted in a larger amplitude localization correction.

8.2.3 Phase coherence length

For an introduction into the behaviour of the phase coherence length as a function of temperature see Section 7.3.4 on page 138.

Takagaki et al [89T6] studied the phase coherence length in arrays of few parallel GaAs wires ($w = 0.10 - 0.66\,\mu$m, $L = 20\,\mu$m, $10 - 20$ parallel wires) fabricated by EBL and ion beam etching. They determined the depletion length by measuring the zero–field conductance as a function of w, extrapolating to $G = 0$. Low–field ($B < 0.01$ T) MR data was compared with 1D weak–localization theory and l_φ as a function of temperature was extracted for $1.5\,\mathrm{K} < T < 4.2\,\mathrm{K}$ (Figs. 224 and 225). For $w = 0.66\,\mu$m, Takagaki et al found $l_\varphi \propto T^{-1/2}$, while in narrower wires $l_\varphi \propto T^{-1/4}$. The temperature dependence of l_φ in a $0.30\,\mu$m wide wire changed around 2.6 K, probably due to a dimensional crossover. The dominant scattering mechanism was electron–electron scattering. Takagaki et al attributed the change of the temperature exponent to a dimensional crossover of the electron–electron scattering from 1D to 2D. Finally, they compared the amplitude of AB oscillations in a ring fabricated of the same wafer with predictions following from the measured l_φ.

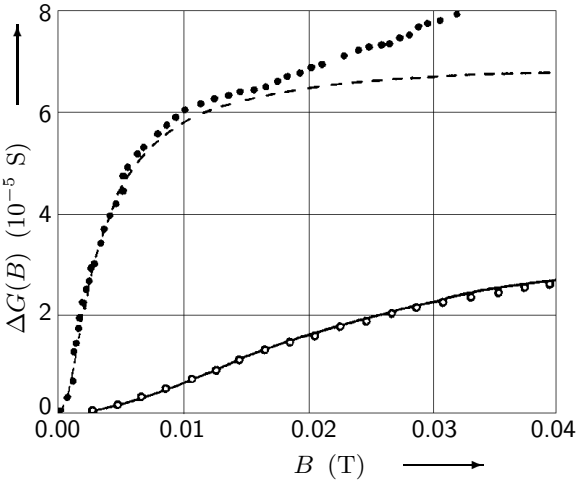

Fig. 224: Low–field MC of $20\,\mu$m long wires at $T = 1.5$ K for $w = 0.66\,\mu$m (top, solid circles) and $w = 0.10\,\mu$m (bottom, open circles) [89T6]. Dashed and solid lines are fits to 1D weak–localization theory.

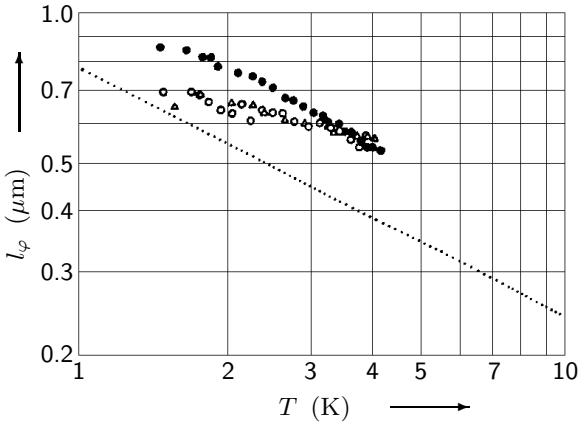

Fig. 225: Temperature dependence of the phase coherence length for $w = 0.66\,\mu$m (solid circles), $w = 0.10\,\mu$m (open circles), and $w = 0.05\,\mu$m (open triangles) [89T6]. The dotted line represents the thermal diffusion length which determines the dimensionality of the electron–electron scattering.

Yamada et al [89Y] investigated arrays of buried on–facet channels. GaAs bars were grown on a semi–insulating substrate and then covered by a $0.01\,\mu$m thick spacer and a $0.1\,\mu$m thick Si–doped $Al_xGa_{1-x}As$ layer. The 2DEG location was determined from angular–dependent SdH oscillations. In type–A samples, the 2DEG was located on the top interface ($w = 0.3\,\mu$m, $L = 50\,\mu$m, $l = 0.7\,\mu$m, 20 parallel channels) and in type–B samples it was located on both sidewall interfaces ($w = 0.6\,\mu$m, $L = 20\,\mu$m, $l = 0.1\,\mu$m, 30 parallel channels). The inelastic scattering length as a function of temperature was extracted from MC measurements via weak–localization theory (Fig. 226): $l_\varphi \propto T^{-0.2}$ (sample A) and $l_\varphi \propto T^{-0.25}$ (sample B). The origin of the small negative power in the temperature dependence was not clear. Yamada et al further measured MC as a function of magnetic field in short single wire samples and observed reproducible conductance oscillations. They investigated the angular dependence of these oscillations.

Potts et al [90P2] (page 241) performed four–terminal magneto transport experiments on (A)

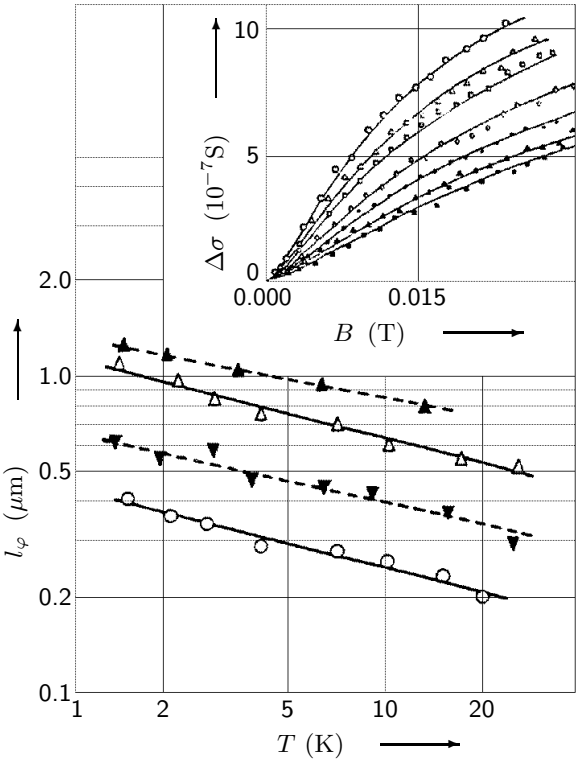

Fig. 226: Temperature dependence of the phase coherence length: raw data of sample A (open upward triangles), corrected data of sample A (filled upward triangles and filled downward triangles), and raw data of sample B (open circles) [89Y]. Inset: Positive MC in sample A at temperatures (top) $T = 1.4\,\mathrm{K}$, $2.2\,\mathrm{K}$, $2.8\,\mathrm{K}$, $4.0\,\mathrm{K}$, $7.0\,\mathrm{K}$, $10.0\,\mathrm{K}$, and $26.0\,\mathrm{K}$ (bottom) fitted by 1D localization theory.

thirty parallel free–standing GaAs wires and on (B) thirty parallel supported GaAs wires. The phase coherence length as a function of temperature was extracted: $l_\varphi \propto T^{-0.47}$ (Fig. 239) in sample A and $l_\varphi \propto T^{-0.66}$ in sample B.

Carpi et al [93C1] (page 243) fabricated parallel $40\,\mu$m long GaAs wires, measured the two–terminal MR and extracted the phase coherence length as a function of temperature. They found $l_\varphi \propto T^{-0.33\pm0.04}$, indicating electron–electron interaction with small energy transfers to be the dominant scattering mechanism.

Reulet et al [95R1] (page 243) examined weak localization in ten parallel, quasi–ballistic GaAs wires and extracted the phase coherence length. The temperature dependence $l_\varphi \propto T^{-1/3}$ indicated electron–electron interactions to be the main dephasing mechanism.

Gershenson et al [97G2] (page 247) estimated the phase coherence length from fits to MR data, yielding $l_\varphi = 0.2 \pm 0.05\,\mu$m at $3\,\mathrm{K}$ and $0.05 \pm 0.01\,\mu$m at $30\,\mathrm{K}$ in five parallel $40\,\mu$m long GaAs wires.

Katine et al [98K3] (page 243) investigated l_φ extracted from MR measurements on an array of GaAs wires. For $T = 385\,\mathrm{mK}$, it was $l_\varphi = 9\,\mu$m, $\tau_\varphi = 150 \pm 5\,\mathrm{ps}$, and $w_{\mathrm{eff}} = 725\,\mathrm{nm}$. They examined τ_φ as a function of temperature between $100\,\mathrm{mK}$ and $4.2\,\mathrm{K}$. It saturated below $200\,\mathrm{mK}$.

Khavin et al [98K4] investigated the temperature dependence of the phase coherence length in arrays of 360 GaAs wires ($w = 0.05\,\mu$m, $L = 500\,\mu$m). An overall gate could be used to change the electron density in the wires. In the temperature dependence of the resistance for different gate voltages, a crossover from WL to SL was observed when T decreased below T_0. From a fit of the data for $T > T_0$ using WL theory, the temperature dependence of l_φ was obtained and was found to be in good agreement with theoretical results over the whole temperature range of the WL regime. As T approached T_0, l_φ was flattened and was $2-3$ times smaller than the localization length at T_0. At a magnetic field where WL was completely suppressed, the measured $R(T)$ was in agreement with the theory of quantum corrections due to electron–electron interactions down

to $T \approx 3T_0$.

8.2.4 Current heating

For an introduction into the phenomenon of current heating see Section 7.3.5 on page 142.

Potts et al [91P2, 92K4, 92P2] studied heating by dc electric fields in fourteen parallel, free–standing GaAs wires ($w \approx 0.4\,\mu$m, $L = 17.5\,\mu$m). As the current was raised, the resistance fell, consistent with the wire heating up in the middle (Figs. 227 and 228). Potts et al compared their results with theory (see also [90P3]).

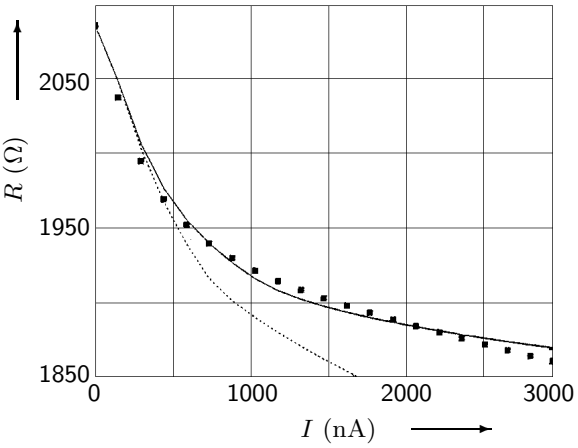

Fig. 227: Resistance vs. heating current: squares are experimental data and solid and dashed lines are two theoretical fits [92P2].

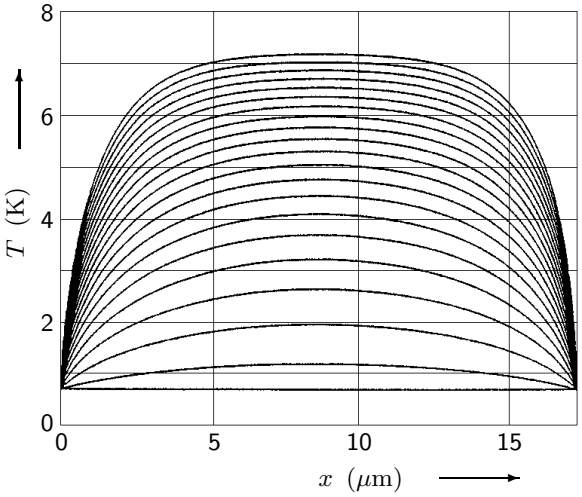

Fig. 228: Temperature profile along the wire for heating currents that rise in steps of 150 nA starting from zero current and rising to 3000 nA [92P2].

8.3 Sample geometry

8.3.1 Width and length

For a short overview over the influence of the width and length of a wire onto its transport properties see Section 7.4.1 on page 144.

Takagaki et al [90T5] studied the width dependence of the MR in ten parallel GaAs wires ($w = 0.2 - 3.0\,\mu$m, $L = 20\,\mu$m) fabricated by EBL and ion etching. The conductance normalized by the number of wires and the channel length was examined. In wide wires, G decreased nearly linearly with w, while it decreased more rapidly in narrower wires. From a linear extrapolation to $G = 0$, a depletion width of $\approx 0.1\,\mu$m was extracted. MR measurements of wires with different widths at 1.5 K showed four contributions (Fig. 229): (1) a negative MR due to weak localization at very small B, (2) SdH oscillations at large B, (3) AF in the whole field range, and (4) a slowly decreasing monotonic negative MR which was enhanced as w became smaller. Takagaki et al examined the electron concentration derived from SdH oscillations as a function of the effective channel width. It was nearly constant in wide wires and decreased suddenly at $w_{\text{eff}} < 1\,\mu$m. The amplitude of the SdH oscillations was suppressed as the channel width decreased. The elastic scattering time was extracted from the data. It was almost independent of temperature between 1.5 and 4.2 K and it gradually decreased with decreasing channel width.

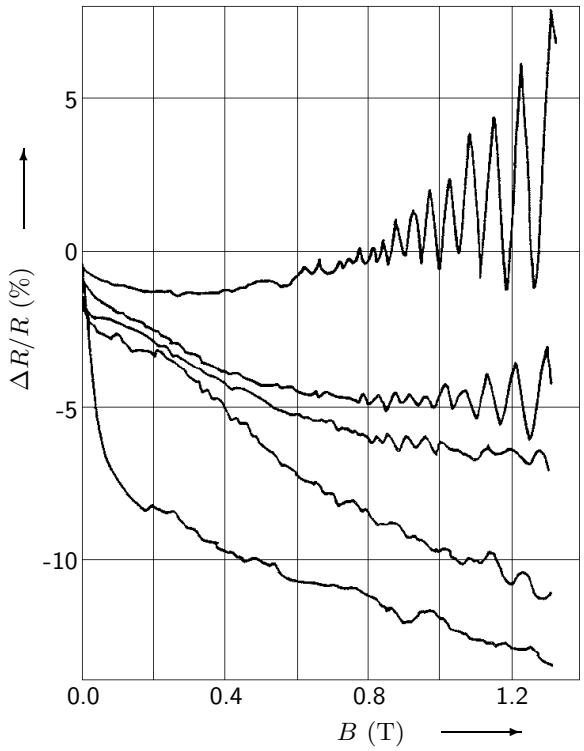

Fig. 229: MR at $T = 1.5\,\mathrm{K}$ and at widths (top) $w = 2.8\,\mu\mathrm{m}$, $1.2\,\mu\mathrm{m}$, $1.0\,\mu\mathrm{m}$, $0.6\,\mu\mathrm{m}$, and $0.3\,\mu\mathrm{m}$ (bottom) [90T5].

Hirler et al [90H] (page 225) measured the dependence of the channel width on gate voltage in arrays of GaAs wires.

Bagwell et al [92B4] (page 241) measured MR in a Si MOSFET. Weak localization at low B was stronger and persisted to larger values of B when the 2DEG was pinched into channels narrower than l_φ.

Mani et al [95M2] (page 245) investigated the two–terminal MR of ≈ 300 parallel GaAs wires. The length variation (for $L = 36$, 57, and $119\,\mu\mathrm{m}$) was examined. At the SdH minima, R approached a length–independent value, while the SdH maxima showed strong length variations.

Hauser et al [94H3] (page 238) investigated transport in arrays of parallel GaAs. The MR was measured for different wire lengths, the deviation from a linear $1/B$ behaviour was independent of wire length.

Katine et al [98K3] (page 243) investigated l_φ extracted from MR measurements on an array of GaAs wires. At $T = 385\,\mathrm{mK}$, $\tau_\varphi = 150 \pm 5\,\mathrm{ps}$ and $w_{\mathrm{eff}} = 725\,\mathrm{nm}$ were extracted assuming specular boundary scattering. Measurements performed for a different channel width yielded $\tau_\varphi = 135\,\mathrm{ps}$ and $w_{\mathrm{eff}} \approx 510\,\mathrm{nm}$.

Maemoto et al [97M] (see page 150) fabricated single and multiple InAs wires with a corrugated surface along the wire and measured MR. Features due to boundary scattering were observed. The channel–length dependence of the I–V characteristic was studied. The high–field electron velocity was estimated from I–V characteristics and was found to increase with decreasing channel width.

8.3.2 Special geometries

The geometry discussed in this Section is a grid–like structure due to perpendicularly intersecting wire arrays.

Smith et al [90S] investigated a GaAs device with a grid–like conducting structure consisting of

0.5 μm long ballistic channels connected both parallel and in series and defined by a gate. The Hall voltage was measured at different gate voltages. At low fields, R_H was quenched for $V_g < -1$ V. At high magnetic fields, the Hall voltage was quantized. The two–terminal MR showed small periodic oscillations which were attributed to the Aharonov–Bohm effect. Smith et al studied conductance vs. gate voltage at different temperatures. The amplitude of sharp peaks in G vs. V_g decreased with increasing magnetic field.

8.4 Impurities

8.4.1 General

For an introduction into the influence of impurities on the transport properties of narrow wires see Section 7.5.1 on page 157 and Section 11.1.4 on page 285.

Skocpol et al [82S1, 83S] (page 228) fabricated fourteen parallel narrow Si MOSFETs and measured the conductance G vs. V_g. Annealing unloaded charged traps and decreased the threshold voltage.

Mani et al [93M3, 94M5] (page 237) performed MR measurements on arrays of GaAs wires and examined various states of disorder using thermal annealing and the persistent photoconductivity effect. Mobility was lower and disorder greater in the shorter wires.

8.4.2 Boundary scattering

For an introduction into the consequences of boundary scattering on transport in small devices see Section 7.5.2 on page 159.

Holzmann et al [94H4] (page 238) performed MR measurements in arrays of parallel Si wires. The two–terminal MR at $T = 0.37$ K showed a maximum for $V_g \leq 0$ V which shifted to larger B and grew in amplitude for lower V_g (Fig. 234). It was attributed to diffusive boundary scattering.

Holzmann et al [95H4, 96H3] (page 238) examined the MR in arrays of $\approx$ 300 Si wires in parallel. A low–field maximum probably due to boundary scattering arose and shifted to higher fields with increasing etch depth.

Hauser et al [94H3] (page 238) investigated transport in arrays of parallel GaAs wires and attributed a maximum in the MR to boundary scattering.

Maemoto et al [97M] (page 233) fabricated single and multiple InAs wires with a corrugated surface along the wire and measured MR. Features due to boundary scattering were observed.

8.5 Interactions

8.5.1 Electron–electron interaction

For an introduction into the influence of electron–electron interactions onto the transport properties of narrow wires see Section 7.6.1 on page 162.

Skocpol et al [82S1, 83S] (page 228) fabricated fourteen parallel narrow Si channels which exhibited a strong variation of conductance with temperature due to a combination of weak localization and interaction effects.

Takagaki et al [89T6] (page 230) studied the phase coherence length in arrays of few parallel GaAs wires (Figs. 224 and 225). The dominant dephasing mechanism was electron–electron scattering.

Potts et al [90P2] (page 241) performed four–terminal magneto transport experiments on (A) thirty parallel free–standing GaAs wires and on (B) thirty parallel supported GaAs wires. The conductance per unit length per wire of sample A varied as $\ln(T)$ due to a combination of 1D weak localization and 3D interaction effects (Fig. 238). MR measurements were performed at different temperatures, the phase coherence length as a function of temperature was extracted, $l_\varphi \propto T^{-0.47}$, characteristic of 3D low–energy electron–electron scattering (Fig. 239). The MR of sample B was measured, the phase coherence length varied as $l_\varphi \propto T^{-0.66}$, indicating again 3D electron–electron interactions.

Mani et al [93M3, 94M5] (page 237) performed MR measurements on arrays of GaAs wires. The results were analysed using temperature power laws characteristic of electron–electron interaction and quantum interference effects.

Carpi et al [93C1] (page 243) fabricated parallel 40 μm long GaAs wires, measured the two–terminal MR, and extracted the phase coherence length as a function of temperature. They found $l_\varphi \propto T^{-0.33\pm0.04}$, indicating electron–electron interaction with small energy transfers to be the dominant scattering mechanism.

Reulet et al [95R1] (page 243) examined weak localization in ten parallel, quasi–ballistic GaAs wires. The phase coherence length was extracted and the temperature dependence, $l_\varphi \propto T^{-1/3}$, indicated electron–electron interactions.

Gershenson et al [97G2] (page 247) measured the temperature dependence of the resistance in five parallel 40 μm long GaAs wires. It was consistent with the theory of quantum corrections due to weak localization and electron–electron interaction effects (Fig. 243).

Katine et al [98K3] (page 243) investigated l_φ extracted from MR measurements on an array of GaAs wires. They assumed electron–electron interaction to be the dominant scattering mechanism.

Khavin et al [98K4] (page 231) studied arrays of GaAs wires. At a magnetic field where WL was completely suppressed, the measured $R(T)$ was in agreement with the theory of quantum corrections due to electron–electron interactions.

Khavin et al [98K5] (page 247) studied the resistance of arrays of GaAs wires. For several samples they repeated the measurements after deposition of a top–gate electrode. The density of states at the Fermi level increased by $\approx 40\%$ after deposition of the gate electrode. The authors attributed this effect to screening of the long–range Coulomb interaction by the metal film.

8.5.2 Electron–phonon interaction

For the general influence of electron–phonon interactions onto transport see Section 7.6.2 on page 165. In the presence of a magnetic field, *magneto–phonon resonances* may be observed, i. e. the magneto conductivity of wide samples shows maxima at those values of magnetic field at which the phonon frequency is an integer multiple of the cyclotron frequency. The maxima occur as, on the one hand, scattering is enhanced when the frequencies are equal and, on the other hand, the current is mainly carried by electron hopping between the localized cyclotron orbits through electron–phonon interaction. In weak confinement potentials, the conductivity also exhibits maxima on resonance. In low–dimensional systems with strong confinement, electrons flow along the edges of the wire. Electron–phonon scattering disturbs this motion and minima in the magneto conductivity are expected whenever an integer multiple of the subband spacing (taking magnetic and 1D geometrical quantization into account) is equal to the phonon energy. This crossover from maxima to minima in the conductivity can either be induced by increasing the curvature of the con-

finement or decreasing the wire width. Hence, information about the geometrical confinement potential may be obtained from the magneto–phonon resonances (see for example [73H, 92M3, 93B4] and references therein).

Berthold et al [93B4] (page 237) performed magneto transport experiments in arrays of parallel GaAs wires. At $T = 106\,\mathrm{K}$, 136 K, and 175 K, structures emerged which were attributed to magneto–phonon scattering (Fig. 231). Below $T = 106\,\mathrm{K}$, the phonon population was too small and above 140 K, the relation $\omega_c\tau > 1$ was not valid, thus the amplitude of the resonance peaks decreased.

Ploner et al [96P1, 97P, 98P2] (page 240) performed magneto–phonon resonance measurements on arrays of forty parallel GaAs wires. The magneto–phonon oscillations depended strongly on the sample structure, the preparation process and the etch depth.

8.6 Magnetic field

8.6.1 General

In this Section, experiments are described in which several magnetic–field dependent phenomena were examined. Experiments in which special phenomena like *weak localization* (see Section 8.6.2 on page 241), *aperiodic conductance fluctuations* (see Section 8.6.3 on page 243), *Shubnikov–de–Haas oscillations* (see Section 8.6.4 on page 244), or the *quantum Hall effect* (see Section 8.6.5 on page 246) were investigated, will be described in the following sub–sections.

Pohlmann et al [86P1] fabricated an array of narrow parallel Si inversion channels ($a = 200\,\mathrm{nm}-20\,\mu\mathrm{m}$) and measured current vs. gate voltage at different magnetic fields. At high B ($\omega_c\tau > 1$), giant oscillations were observed in the MC vs. V_g, the maxima exceeded the $B = 0\,\mathrm{T}$ conductance (Fig. 230). The conductance maxima increased with increasing magnetic field, with decreasing source–drain voltage and with decreasing temperature. The oscillations exceeded the $B = 0\,\mathrm{T}$ conductance only at sufficiently low periodicities a.

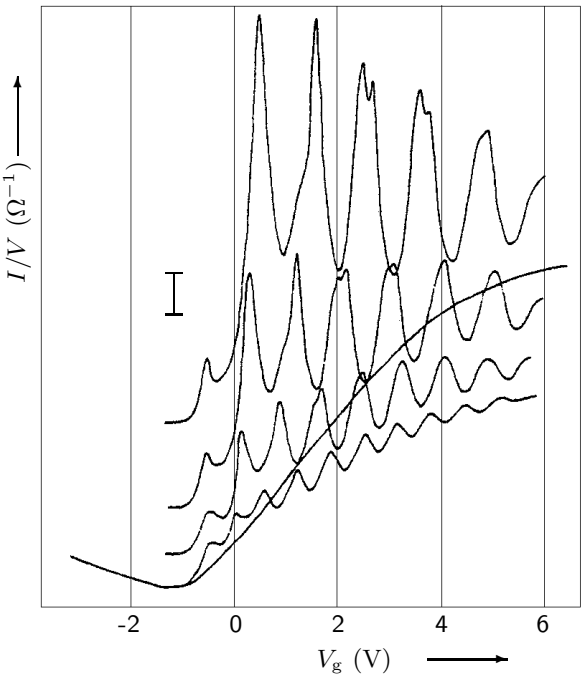

Fig. 230: Two–terminal conductance vs. gate voltage for $a = 260\,\mathrm{nm}$, $T = 1.8\,\mathrm{K}$, and source–drain voltage 25 mV at (top) $B = 11.1\,\mathrm{T}$, 9.5 T, 7.9 T, and 6.3 T (bottom) [86P1]. The vertical bar denotes an amplitude of $10^{-3}\Omega^{-1}$.

Takagaki et al [90T5] (page 232) studied MR in parallel GaAs wire arrays and observed a slowly decreasing monotonic negative MR which was enhanced as w became smaller.

Smith et al [90S] (page 233) investigated a GaAs device with a grid–like conducting structure. The two–terminal MR showed small periodic oscillations which were attributed to the Aharonov–Bohm effect. They further studied conductance vs. gate voltage and the amplitude of sharp peaks in G vs. V_g decreased with increasing magnetic field.

Hirler et al [90H] (page 225) presented measurements of 1D subband energies in arrays of GaAs wires. The subband spacing increased in a magnetic field

Bagwell et al [92B4] (page 241) fabricated a dual gate Si MOSFET with a grating gate (bottom) and a continuous gate (top) and performed various measurements of G vs. top–gate voltage for different magnetic fields. At very large magnetic fields, $B > 20\,\mathrm{T}$, quantized two-terminal conductance emerged.

Gusev et al [93G2] fabricated a lateral superlattice of etched GaAs stripes ($a = 0.6\,\mu$m, $w = 0.15 - 0.2\,\mu$m, $L = 5$ and $10\,\mu$m, $l = 1.5\,\mu$m) in which the regions beneath the stripes were depleted from electrons, but electrons could diffuse between neighbouring wires. The four–terminal MR was measured, it decreased with B. At small B, some features were observed, while SdH oscillations developed at large B. The positions of the maxima depended on the length of the stripes. A negative MR at small B was due to weak localization.

Berthold et al [93B4] performed magneto transport experiments for $2\,\mathrm{K} < T < 175\,\mathrm{K}$ in arrays of parallel GaAs wires fabricated by (A) EBL and subsequent wet chemical etching for 45 s ($a = 600\,$nm, $w = 200\,$nm, $L = 10\,\mu$m) and by (B) holographic lithography and subsequent wet chemical etching for 30 s ($a = 425\,$nm, $w = 200\,$nm, $L = 100\,\mu$m). MR measurements at $T = 3\,\mathrm{K}$ revealed SdH oscillations above $B = 1\,\mathrm{T}$. A Landau plot showed deviations from a linear behaviour and subband spacings of 2.5 meV in sample A and 1.0 meV in sample B were estimated. At $T = 106\,\mathrm{K}$, 136 K, and 175 K, SdH oscillations were absent, but structures emerged which were attributed to magneto–phonon scattering (Fig. 231). Below $T = 106\,\mathrm{K}$, the phonon population was too small and above 140 K, the relation $\omega_c\tau > 1$ was not valid, thus the amplitude of the resonance peaks decreased. Subband spacings determined from the magneto–phonon resonances were 7.2 meV in sample A and 2.6 meV in sample B. Berthold et al concluded that temperature influenced the shape of the confining potential.

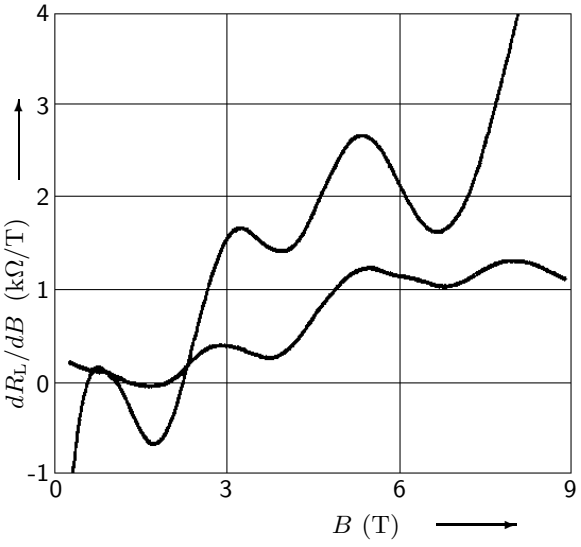

Fig. 231: Derivative of resistance, dR_L/dB, of sample A at $T = 136\,\mathrm{K}$ (right, top) and at $T = 175\,\mathrm{K}$ (right, bottom) [93B4].

Mani et al [93M3, 94M5] performed MR measurements on arrays of GaAs wires ($a = 730\,$nm,

$w = 400\,\mathrm{nm}$, $w_{\mathrm{eff}} < 200\,\mathrm{nm}$, $L = 77$ and $98\,\mu\mathrm{m}$) fabricated by holographic lithography and shallow etching. Various states of disorder were examined using thermal annealing and the persistent photoconductivity effect. Mobility was lower and disorder greater in the shorter wires. Localization lengths of $8.5\,\mu\mathrm{m}$ and $9.5\,\mu\mathrm{m}$ were estimated for the 77 and the $98\,\mu\mathrm{m}$ long wires, respectively. A resistance peak in the MR at $B = 0\,\mathrm{T}$ increased with decreasing T. At $B = 300\,\mathrm{mT}$, the resistance of the $77\,\mu\mathrm{m}$ long wire increased by a factor of 3.4 upon reducing T from 1.2 to 0.05 K, while the resistance of the $98\,\mu\mathrm{m}$ long wire changed by a factor of 1.6 (Figs. 232 and 233). The results were analysed using temperature power laws which were characteristic of electron–electron interaction and quantum interference effects. At 1.2 K, both wires showed 1D behaviour, at lower T the $98\,\mu\mathrm{m}$ long wire showed 0D behaviour as far as both localization and interaction effects were concerned, while the $77\,\mu\mathrm{m}$ long wire showed mixed dimensionality.

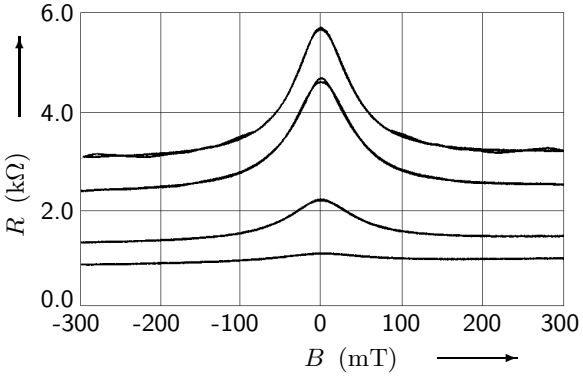

Fig. 232: Low–field MR in the $77\,\mu\mathrm{m}$ long wires at (top) $T = 0.05\,\mathrm{K}$, 0.10 K, 0.30 K, and 1.20 K (bottom) [93M3].

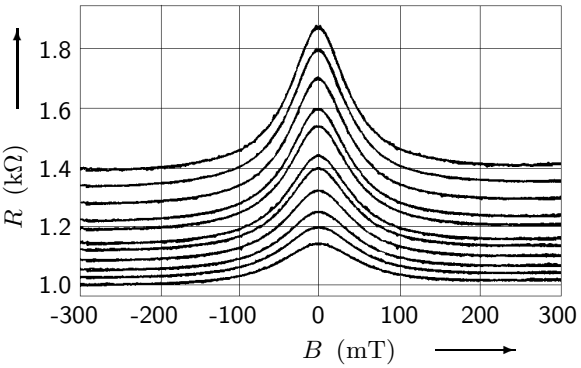

Fig. 233: Low–field MR in the $98\,\mu\mathrm{m}$ long wires at (top) $T = 0.05\,\mathrm{K}$, 0.10 K, 0.19 K, 0.31 K, 0.42 K, 0.49 K, 0.62 K, 0.81 K, 1.00 K, 1.20 K, and 1.51 K (bottom) [93M3].

Holzmann et al [94H4] performed MR measurements in arrays of parallel Si wires ($a = 1.3\,\mu\mathrm{m}$, $w = 0.5\,\mu\mathrm{m}$, $L = 450\,\mu\mathrm{m}$) defined by holographic lithography and wet chemical etching. The two–terminal MR for $-1.2\,\mathrm{V} < V_{\mathrm{g}} < 0.5\,\mathrm{V}$ at $T = 0.37\,\mathrm{K}$ showed a maximum for $V_{\mathrm{g}} \leq 0\,\mathrm{V}$ which shifted to larger B and grew in amplitude for lower V_{g} (Fig. 234). It did not depend on temperature (Fig. 235). At $V_{\mathrm{g}} = 0.5\,\mathrm{V}$, the maximum was not observable. This low–field maximum was attributed to diffusive boundary scattering. MR oscillations resembled SdH oscillations. A Landau plot showed no deviation from a linear behaviour.

Holzmann et al [95H4, 96H3] fabricated arrays of ≈ 300 Si wires in parallel ($a = 480\,\mathrm{nm}$, $L = 20 - 150\,\mu\mathrm{m}$ and $L = 300\,\mu\mathrm{m}$, $l = 1.7\,\mu\mathrm{m}$) by shallow and deep RIE and measured the two–terminal MR at $T = 360 \pm 10\,\mathrm{mK}$. The sample with an etch depth of $d = 50\,\mathrm{nm}$ showed 2D transport characteristics, well–pronounced plateaux due to the QHE were observed in the MR down to filling factor $\nu = 36$. The shape of the MR changed when d became larger. A low–field maximum probably due to boundary scattering arose and shifted to higher fields with increasing d. Landau plots showed deviations from linear behaviour, demonstrating the existence of 1D subbands (Fig. 236). The subband spacing, $\hbar\omega_0 = 0.3 - 1.0\,\mathrm{meV}$, the 1D carrier density, and the effective wire width, $w_{\mathrm{eff}} = 70 - 180\,\mathrm{nm}$, were extracted. In the smallest wire, only four subbands were occupied.

Hauser et al [94H3] investigated transport in arrays of parallel GaAs wires defined by holographic gratings (sample A: $a = 300\,\mathrm{nm}$, $w = 200\,\mathrm{nm}$, $L = 100\,\mu\mathrm{m}$) followed by a step–wise wet chemical etch in order to create different heights of the 1D confinement potential, and by EBL (sample B: $a = 600\,\mathrm{nm}$, $w = 200\,\mathrm{nm}$, $L = 1 - 20\,\mu\mathrm{m}$) and subsequent wet chemical etching. The MR in sample A was measured at different etch steps (at $T = 1.8\,\mathrm{K}$), a maximum due to boundary

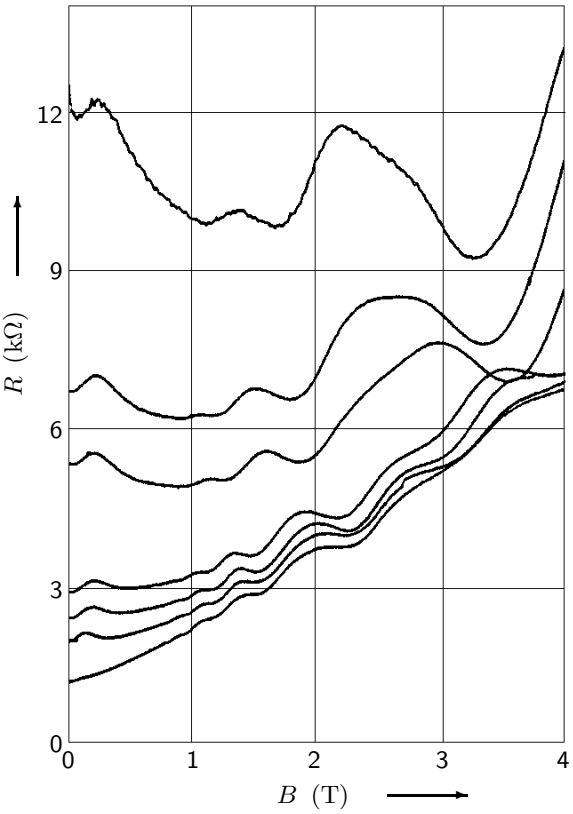

Fig. 234: Two–terminal MR parallel to the wires at $T = 370\,\mathrm{mK}$ and gate voltages (top) $V_\mathrm{g} = -1200\,\mathrm{mV}$, $-1000\,\mathrm{mV}$, $-800\,\mathrm{mV}$, $-600\,\mathrm{mV}$, $-400\,\mathrm{mV}$, $0\,\mathrm{mV}$, and $500\,\mathrm{mV}$ (bottom) [94H4].

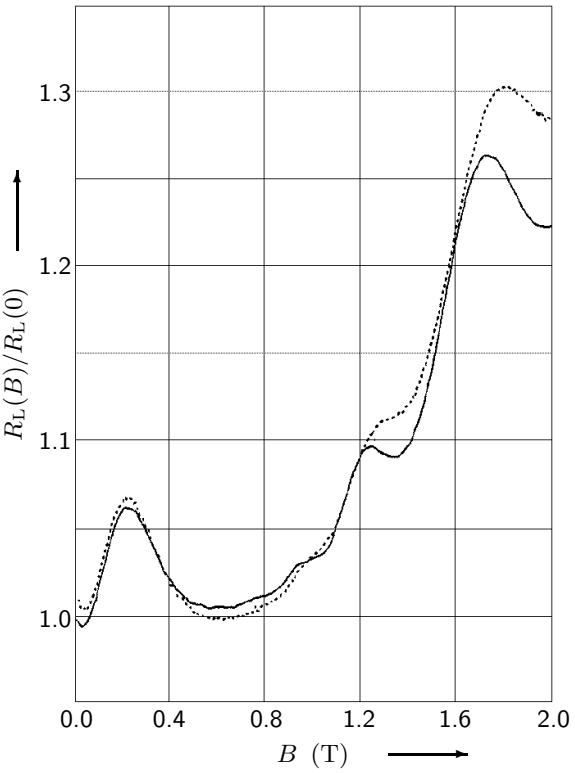

Fig. 235: Temperature–dependent MR at $V_\mathrm{g} = -0.7\,\mathrm{V}$ and $T = 0.37\,\mathrm{K}$ (solid curve) and $T = 1.2\,\mathrm{K}$ (dashed curve) [94H4]. The backscattering peak's position at $\approx 0.2\,\mathrm{T}$ and its amplitude remained unaffected.

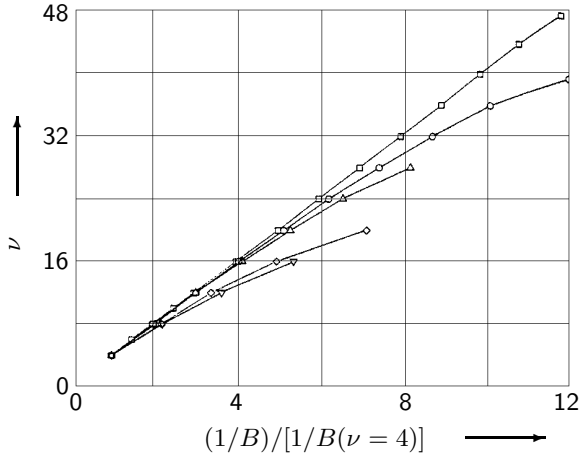

Fig. 236: Filling factors ν vs. $(1/B)/[1/B(\nu = 4)]$ for etch depths (top, squares) 50 nm, 55 nm (circles), 60 nm (upward triangles), 85 nm (diamonds), and 92 nm (downward triangles, bottom) [95H4].

scattering was found at $B = 0.8$ T. Increasing the confinement potential resulted in a negative differential MR. SdH oscillations were observed, Landau plots deviated from a linear $1/B$ dependence at the last two etch steps. The MR of sample B was measured for different wire lengths, the deviation from a linear $1/B$ behaviour was independent of wire length. The 1D electron density, the height of the confinement potential and the effective width were obtained from the Landau plots. Hauser et al further examined the I–V characteristic of sample A. Deviations from a linear ohmic behaviour were found at small electric fields which became more pronounced with increasing etch depth (Fig. 237). At higher electric fields, the I–V characteristic became linear. The differential resistance decreased with increasing electric field and increased with the etch depth. The mobility was extracted from the data and analysed in terms of external parameters. The mobility of sample B was also studied. Finally, Hauser et al measured the drift velocity as a function of electric field at different etch depths.

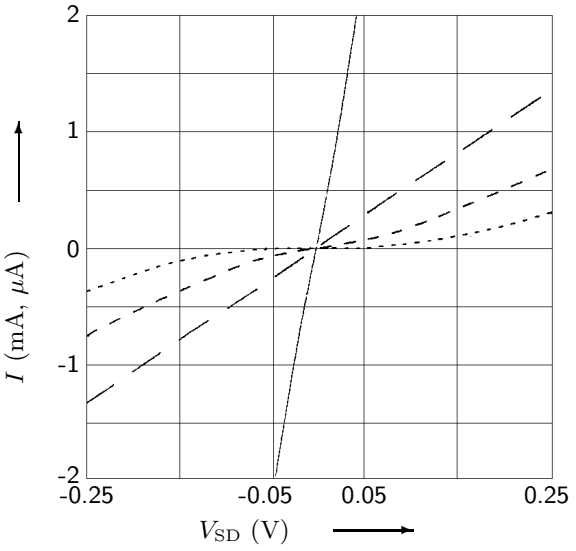

Fig. 237: I–V characteristics at $T = 1.8$ K for a 2DEG (solid line, left axis in mA) and etching times of 25 s (long dashes, left axis in mA), 35 s (short dashes, left axis in μA), and 40 s (dots, left axis in μA) [94H3].

Ploner et al [96P1, 97P, 98P2] performed magneto–phonon resonance studies on arrays of forty parallel GaAs wires fabricated by laser holography and wet chemical etching. The wires were completely depleted at 4.2 K, electron density was varied by illumination with a LED. The samples were heated to $100 - 160$ K, MPR measurements were performed, then the samples were cooled to 2 K and magnetic depopulation measurements were performed. The magneto–phonon oscillations depended strongly on the sample structure, the preparation process and the etch depth. In order to observe sufficiently pronounced MPR, the authors were restricted to a relatively weak confinement and low electron densities. Magnetic depopulation measurements gave a non–linear behaviour of the subband index n vs. $1/B$, displaying the 1D behaviour, and subband spacings of 1.1 ± 0.2 meV were deduced. MPR measurements were in accordance with theory, the relation between B^2 and $1/n^2$ was linear, a subband spacing of 1.6 ± 0.3 meV was deduced. Ploner et al explained the difference between the subband spacings via the deviation of the actual confinement potential from a parabolic shape. The theoretical fits yielding the subband spacings were based on a parabolic confinement. Further, they investigated the dependence of the subband spacing on the electron density via MPR measurements.

Gershenson et al [97G2] (page 247) reported observation of a crossover from weak to strong localization in five parallel 40 μm long GaAs wires. Features of the MR in the regime of strong localization were in accordance with a doubling of the localization length in quasi 1D conductors in a strong magnetic field. Further, Gershenson et al examined the magnetic–field dependence of the activation energy.

Katine et al [98K3] (page 243) investigated weak localization and a gradual negative MC in an array of GaAs wires. At $B \approx 80\,\mathrm{mT}$, the MC became positive.

Maemoto et al [97M] (page 233) fabricated single and multiple InAs wires with a corrugated surface along the wire and measured MR. Features due to boundary scattering were observed.

Khavin et al [98K5] (page 247) studied the resistance of arrays of GaAs wires. The MR in the WL and the SL regime was negative and strongly anisotropic. The crossover between WL and SL shifted to lower temperatures in weak magnetic fields. The activation energy changed with magnetic field and thus the localization length ξ. The localization length doubled at a characteristic field due to breaking of the time–reversal symmetry.

8.6.2 Weak localization

For an introduction into the phenomenon of weak localization see Section 7.7.2 on page 176.

Skocpol et al [82S1, 83S] (page 228) fabricated fourteen parallel narrow Si channels which exhibited a strong variation of conductance with temperature due to a combination of weak localization and interaction effects.

Alsmeier et al [88A] (page 244) measured MR of multi–wire inversion channels on InSb. In dR/dV_g vs. B, structure attributed to weak localization was visible.

Takagaki et al [89T6] (page 230) measured low–field MR in arrays of few parallel GaAs wires, compared the data with 1D weak–localization theory, and extracted l_φ as a function of temperature (Figs. 224 and 225).

Yamada et al [89Y] (page 230) extracted the inelastic scattering length as a function of temperature from MC measurements on buried on–facet channels via weak–localization theory (Fig. 226).

Takagaki et al [90T5] (page 232) studied the MR of parallel GaAs wire arrays and observed a negative MR due to weak localization at small B.

Potts et al [90P2] performed four–terminal magneto transport experiments on (A) thirty parallel free–standing GaAs wires ($w = 600\,\mathrm{nm}$, $L = 3.2\,\mu\mathrm{m}$) and on (B) thirty parallel supported GaAs wires ($w = 900\,\mathrm{nm}$, $L = 10\,\mu\mathrm{m}$). The conductance per unit length per wire of sample A varied as $\ln(T)$ over the range $0.47\,\mathrm{K} < T < 10.0\,\mathrm{K}$ due to a combination of 1D weak localization and 3D interaction effects (Fig. 238). MR measurements were performed at different temperatures in magnetic fields up to 0.15 T and the data was fitted by 1D weak–localization theory. The phase coherence length as a function of temperature was extracted, $l_\varphi \propto T^{-0.47}$, characteristic of 3D low–energy electron–electron scattering (Fig. 239). The MR of sample B was measured for $0.47\,\mathrm{K} < T < 4.2\,\mathrm{K}$ and $-0.15\,\mathrm{T} < B < 0.15\,\mathrm{T}$ and the data was fitted by 3D weak–localization theory. The phase coherence length varied as $l_\varphi \propto T^{-0.66}$, indicating again 3D electron–electron interactions.

Bagwell et al [92B4] fabricated a dual gate Si MOSFET with a grating gate (bottom, $a = 200\,\mathrm{nm}$) and a continuous gate (top). They measured conductance vs. top–gate voltage for various bottom–gate voltages and observed a feature in the curves at gate voltage configurations at which the electron gas was confined beneath the grating wires (Fig. 240). At values of the bottom–gate voltage, for which the electron gas was confined in the gaps between the grating lines for any value of the top–gate voltage, this feature was missing. Weak localization at low B was stronger and persisted to larger values of B when the 2DEG was pinched into channels narrower than l_φ. Bagwell et al performed various measurements of G vs. top–gate voltage for different bottom–gate voltages, different magnetic fields, and different temperatures. At very large magnetic fields, $B > 20\,\mathrm{T}$, quantized two-terminal conductance emerged.

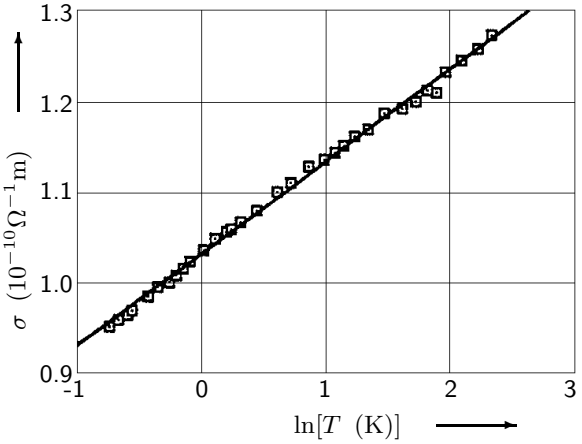

Fig. 238: Plot of 1D conductivity per wire vs. $\ln(T)$ [90P2].

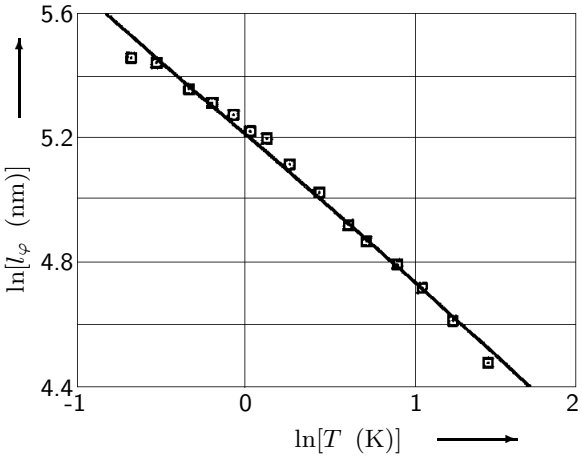

Fig. 239: Double–logarithmic plot of the phase coherence length as a function of temperature [90P2].

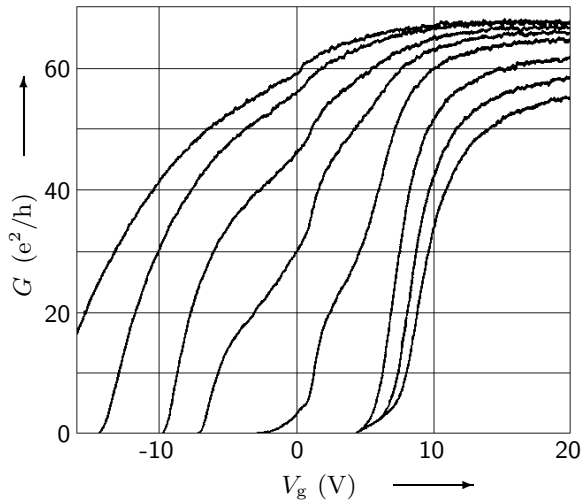

Fig. 240: I–V characteristic at $B = 0\,\mathrm{T}$ and $T < 50\,\mathrm{mK}$ vs. top–gate voltage for bottom–gate voltages of (left) 5 V, 4 V, 3 V, 2.5 V, 2 V, 1 V, 0 V, and -1 V [92B4]. The five curves on the left show a kink near 0 V, while no such kink is observed in the three rightmost curves.

Kurdak et al [92K1] studied rings and wire arrays of $GaAs/Al_{0.3}Ga_{0.7}As$ and pseudomorphic $Ga_{0.2}I_{0.8}As/Al_{0.48}In_{0.52}As$ modulation–doped heterostructures. In the parallel wires, l_φ was deduced from weak–localization measurements (see page 256).

Gusev et al [93G2] (page 237) examined a lateral superlattice of etched GaAs stripes. The four–terminal MR was measured and a negative MR at weak B was due to weak localization.

Carpi et al [93C1] fabricated parallel 40 μm long GaAs wires ((A) $w = 1\,\mu$m, 45 wires; (B) $w = 0.8\,\mu$m, 52 wires; (C) $w = 0.56\,\mu$m, 60 wires) by EBL and RIE and measured the two–terminal MR. The data was fitted by 1D weak–localization theory and the phase coherence length as a function of temperature was extracted. Carpi et al found $l_\varphi \propto T^{-0.33\pm0.04}$, indicating electron–electron interaction with small energy transfers to be the dominant scattering mechanism.

Reulet et al [95R1] examined weak localization in ten parallel, quasi–ballistic GaAs wires ($w = 0.3$, 0.5, and 0.88 μm, $L = 100\,\mu$m). The negative MR peak became sharper with decreasing temperature. Superimposed on the MR, AF were observed whose amplitude increased with decreasing T. The data was compared with theory, the effective width and the phase coherence length were extracted. The temperature dependence $l_\varphi \propto T^{-1/3}$ indicated electron–electron interactions.

Gershenson et al [97G2] (page 247) reported observation of a crossover from weak to strong localization in five parallel 40 μm long GaAs wires. The temperature dependence of the resistance was consistent with the theory of quantum corrections due to weak localization and electron–electron interaction effects at high enough T (Fig. 243).

Katine et al [98K3] investigated l_φ extracted from MR measurements on an array (four identical columns in series, each consisting of five parallel channels) of GaAs wires ($w = 800$ nm, $L = 105\,\mu$m) defined by a split gate. The gate voltage was -400 mV, weak localization and a gradual negative MC were observed in a four–probe measurement. At higher fields (≈ 80 mT), the MC became positive. At a temperature of $T = 385$ mK, $l_\varphi = 9\,\mu$m, $\tau_\varphi = 150 \pm 5$ ps, and $w_{\text{eff}} = 725$ nm were extracted assuming specular boundary scattering. Lower temperatures resulted in a larger amplitude localization correction. Katine et al examined τ_φ as a function of temperature between 100 mK and 4.2 K. It saturated below 200 mK. They assumed electron–electron interaction to be the dominant scattering mechanism. Measurements performed for a different channel width (accomplished by changing the gate voltage) yielded $\tau_\varphi = 135$ ps and $w_{\text{eff}} \approx 510$ nm at $V_g = -1000$ mV.

8.6.3 Aperiodic conductance fluctuations

For an introduction into the phenomenon of aperiodic fluctuations of conductance as a function of magnetic field see Section 7.7.3 on page 182.

Yamada et al [89Y] (page 230) measured MC as a function of magnetic field in short single mesa–shaped bar samples and observed reproducible conductance fluctuations. They investigated the angular dependence of these fluctuations.

Takagaki et al [90T5] (page 232) measured the MR of parallel GaAs wire arrays and observed AF.

Reulet et al [95R1] (page 243) examined weak localization in ten parallel, quasi–ballistic GaAs wires. Superimposed on a negative MR, AF were observed whose amplitude increased with decreasing T.

Gershenson et al [97G2] (page 247) observed AF whose amplitude increased with decreasing temperature in five parallel 40 μm long GaAs wires.

8.6.4 Shubnikov–de–Haas oscillations

For an introduction into the phenomenon of Shubnikov–de–Haas oscillations see Section 7.7.4 on page 194.

Grassie et al [87G2] (see page 195) studied SdH oscillations in nine parallel GaAs wires and analysed their amplitudes.

Brinkop et al [88B1] studied MR in an array of $\approx$ 7000 parallel GaAs wires ($a = 400\,\mathrm{nm}$) defined for gate voltages below $-0.5\,\mathrm{V}$ on a holographically defined gate. For $B > 0.5\,\mathrm{T}$, quantum oscillations became visible. A fan diagram (index of oscillation maxima vs. $1/B$) showed a deviation from a linear 2D behaviour at low magnetic fields, reflecting quantization of the electronic motion by the lateral confining potential.

Alsmeier et al [88A] measured MR of multi–wire inversion channels on InSb ($a = 250\,\mathrm{nm}$, $w \approx 100\,\mathrm{nm}$). Free electrons were induced by a positive voltage on a homogeneous gate. The resistance R and dR/dV_g were measured for a current parallel and perpendicular to the channels. No conductivity was observed in the perpendicular geometry. In dR/dV_g vs. B, oscillations due to 1D subband depopulation (subband spacing $\approx 10\,\mathrm{meV}$) were observed. At very weak magnetic field, structure attributed to weak localization was visible. At $B \approx 4-5\,\mathrm{T}$, SdH oscillations arising from the 2D regions between the grating and the contact areas were observed.

Demel et al [88D] (page 224) investigated shallow etched (A) and deep etched (B) GaAs single–layer quantum wire arrays and a deep etched (C) GaAs double–layer quantum wire array. Magneto transport measurements revealed SdH oscillations with a period non–linear in $1/B$ in sample A (Fig. 217). In the quasi–dc conductivity of samples B and C (measured by microwave transmission), SdH oscillations also showed a deviation from a linear $1/B$ behaviour (Figs. 218 and 219).

Merkt [89M5] (page 224) performed MR measurements on parallel InSb and GaAs wires and observed SdH oscillations. Landau plots deviated from a straight line.

Yamada et al [89Y] (page 230) investigated arrays of buried on–facet channels and determined the location of the 2DEG from angular–dependent SdH oscillations.

Takagaki et al [90T5] (page 232) measured MR of parallel GaAs wire arrays and observed SdH oscillations at large B. They examined the electron concentration derived from SdH oscillations as a function of the effective channel width. The amplitude of the SdH oscillations was suppressed as the channel width decreased.

Kern et al [90K3] (page 225) fabricated wire arrays on InGaAs, performed quasi–dc magneto-transport experiments at 2.2 K, and observed SdH oscillations. The index of the oscillations did not depend linearly on $1/B$ at small B, demonstrating a 1D confined energy spectrum.

Gao et al [90G3] (page 226) examined MR in 240 parallel Si wires defined by a gate. The dependence of $\partial G/\partial V_\mathrm{g}$ on magnetic field (for fields up to 20 T) showed oscillations attributed to the SdH effect. The positions of the maxima vs. $1/B$ deviated from a linear behaviour at small B.

Hirler et al [90H] (page 225) measured magneto transport in arrays of GaAs wires. The differential MR, dR/dV_g, was measured as a function of magnetic field and a Landau plot of MR oscillations showed deviations from a linear behaviour in $1/B$, indicating the existence of 1D subbands.

Demel et al [91D] (page 225) performed magneto transport measurements on parallel GaAs wires. The MR (at $T = 2.2\,\mathrm{K}$) exhibited SdH oscillations and Landau plots deviated from a linear behaviour, indicating the formation of 1D subbands.

Mani et al [92M2, 94M5] fabricated arrays of parallel GaAs wires ($a = 730\,\mathrm{nm}$, $w = 400\,\mathrm{nm}$, $w_\mathrm{eff} = 130 - 200\,\mathrm{nm}$, $L = 98\,\mu\mathrm{m}$, $l \approx 1.4\,\mu\mathrm{m}$, ≈ 260 electrically active wires) by holographic lithography and plasma etching. The two–terminal MR exhibited SdH oscillations (Fig. 241).

The extrema positions as a function of $1/B$ deviated from a linear behaviour (confinement energy $0.5-1.0\,\mathrm{meV}$, $7-11$ subbands occupied). The amplitude of the SdH oscillations showed a stronger temperature dependence with increasing B. In the four–terminal resistance, the SdH linewidth narrowed on the high–field side of the oscillations with decreasing temperature and remained relatively unaffected by T on the low–field side. This feature was reproduced in different samples with increasing lengths up to $120\,\mu\mathrm{m}$. Mani et al examined the half width at half maximum on the high–field side of the SdH peak, ΔB, as a function of temperature and found $\Delta B \propto T^{0.4(\pm 3\%)}$. They interpreted their results in terms of temperature–induced electronic localization.

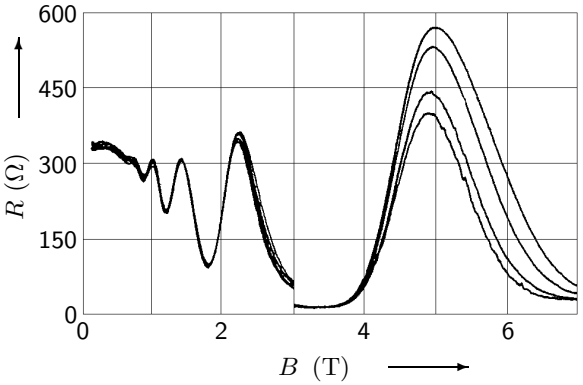

Fig. 241: Two–terminal resistance as a function of magnetic field in $98\,\mu\mathrm{m}$ long wires at (peak at 5 T, left) $T = 0.220\,\mathrm{K}$, $0.430\,\mathrm{K}$, $0.730\,\mathrm{K}$, and $1.000\,\mathrm{K}$ (peak at 5 T, right) [92M2]. From 3 T to 7 T the data was reduced by a factor of 3.

Gusev et al [93G2] (page 237) examined a lateral superlattice of etched GaAs stripes. SdH oscillations were observed at large B, the positions of the maxima depended on the length of the stripes.

Berthold et al [93B4] (page 237) performed magneto transport experiments in arrays of parallel GaAs wires and observed SdH oscillations at $T = 3\,\mathrm{K}$ above $B = 1\,\mathrm{T}$. A Landau plot showed deviations from a linear behaviour. At $T = 106\,\mathrm{K}$, $136\,\mathrm{K}$ and $175\,\mathrm{K}$, SdH oscillations were absent.

Motohisa et al [93M4] fabricated 100 parallel GaAs wires ($w = 100\,\mathrm{nm}$) by cleaved edge overgrowth. At 4.2 K, the sample did not conduct without illumination. Red light of a LED was used to make the sample conductive, increasing the light intensity decreased the sample resistance. The MR was measured at different angles ($\theta = 0°$ and $\theta = \pm 41.5°$) and MR oscillations were observed. The positions of peaks and valleys followed $B \propto 1/\cos(\theta)$. A Landau plot showed deviation from a straight line, demonstrating the quasi 1D nature of the electronic states (subband spacing $\approx 2.2\,\mathrm{meV}$, five subbands occupied at $B = 0\,\mathrm{T}$.)

Mani et al [95M2] investigated the two–terminal MR of parallel GaAs wires ($a = 730\,\mathrm{nm}$, $w = 400\,\mathrm{nm}$, $w_{\mathrm{eff}} = 200\,\mathrm{nm}$, $L = 57\,\mu\mathrm{m}$) fabricated by shallow plasma etching. SdH oscillations were observed, the low–ν minima showed a non–zero slope in R (Fig. 242). The SdH minima saturated to a temperature–independent behaviour in the vicinity of $\nu = 1$ and $\nu = 2$ at low T. At larger temperatures, $1.5\,\mathrm{K} \le T \le 5\,\mathrm{K}$, a $\nu = 1$ resistance minimum in a $810\,\mathrm{nm}$ period sample revealed localization and activated transport. The length variation of the two–terminal resistance (for $L = 36$, 57, and $119\,\mu\mathrm{m}$) was examined. At the SdH minima, R approached a length–independent value, while the SdH maxima showed strong length variations. Mani et al discussed their observations in terms of the Hall effect.

Holzmann et al [94H4] (page 238) performed MR measurements in arrays of parallel Si wires. MR oscillations resembled SdH oscillations and a Landau plot showed no deviation from a linear behaviour.

Holzmann et al [95H4, 96H3] (page 238) examined MR in arrays of ≈ 300 Si wires in parallel. Landau plots showed deviations from linear behaviour, demonstrating the existence of 1D subbands (Fig. 236).

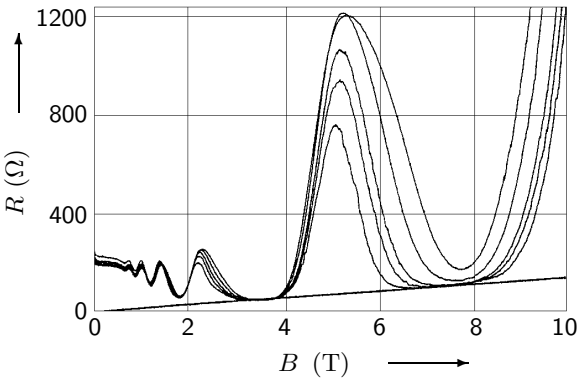

Fig. 242: Two–terminal resistance vs. magnetic field at temperatures (peak at 5 T, left) $T = 0.04$ K, 0.21 K, 0.41 K, 0.80 K, and 1.37 K (peak at 5 T, right) [95M2]. A tangent line connects the origin with the $\nu = 1$ and $\nu = 2$ minima.

Hauser et al [94H3] (page 238) investigated transport in arrays of parallel GaAs wires. SdH oscillations were observed and Landau plots deviated from a linear $1/B$ dependence.

Ploner et al [96P1, 97P, 98P2] (page 240) performed magneto–phonon resonance studies on arrays of forty parallel GaAs wires, then cooled the samples to 2 K and performed magnetic depopulation measurements.

Sasa et al [96S1] (page 226) fabricated arrays of ten parallel wires of InAs/AlGaSb, performed MR measurements for $0\,\mathrm{T} < B < 8\,\mathrm{T}$ at 4.2 K and observed SdH oscillations. Landau plots showed deviations from a linear behaviour for all samples.

Friedland et al [99F2] (page 227) realized an array of a few quantum wires utilizing multiatomic step arrays at the interface of GaAs/AlGaAs heterostructues. SdH oscillation measurements revealed independent conductance along the parallel wires and 1D confinement.

8.6.5 Quantum Hall effect

For an introduction into the phenomenon of *quenching* of the Hall resistance see Section 7.7.5 on page 200.

Smith et al [90S] (page 233) investigated a GaAs device with a grid–like conducting structure and measured the Hall voltage at different gate voltages. At low fields, R_H was quenched for $V_\mathrm{g} < -1$ V while at high magnetic fields, the Hall voltage was quantized.

Holzmann et al [95H4, 96H3] (page 238) examined the MR in arrays of ≈ 300 Si wires in parallel. Plateaux due to the QHE were observed in the MR down to filling factor $\nu = 36$.

8.7 Non–linear effects

For an introduction into the phenomenon of a non–linear current–voltage characteristic see Section 7.9 on page 210.

Potts et al [88P] fabricated arrays of free–standing Si wires ($w = 0.6\,\mu$m, $L = 40\,\mu$m) by EBL and plasma etching. Preliminary electrical measurements carried out at room temperature revealed non–ohmic behaviour with a dc resistance of $\approx 10\,\mathrm{M}\Omega$. The wires were sensitive to heating and direct illumination.

Hauser et al [94H3] (page 238) investigated transport in arrays of parallel GaAs wires defined by holographic gratings followed by a step–wise wet chemical etch. The I–V characteristic deviated from a linear ohmic behaviour at small electric fields. The deviation became more pronounced with increasing etch depth. At higher electric fields, the I–V characteristic became linear.

Khavin et al [98K5] (page 247) studied the resistance of arrays of GaAs wires. The non–linear I–V characteristics was measured at different temperatures.

8.8 Localization

For an introduction into the phenomenon of localization see Section 7.10 on page 212.

Mani et al [92M2, 94M5] (page 244) measured MR in arrays of parallel GaAs wires. In the four–terminal resistance, the SdH linewidth narrowed on the high–field side of the oscillations with decreasing temperature and remained relatively unaffected by T on the low–field side. They examined the half width at half maximum on the high–field side of the SdH peak as a function of temperature and interpreted their results in terms of temperature–induced electronic localization.

Hasko et al [93H2] (page 228) reported fabrication of eight parallel free–standing GaAs wires defined by wet etching and overgrowth and found that the resistance depended strongly on temperature, characteristic of hopping conduction. Below 1 K, a transition from 3D to 1D hopping was observed.

Mani et al [93M3, 94M5] (page 237) performed MR measurements on arrays of GaAs wires. Localization lengths of 8.5 μm and 9.5 μm were estimated for a 77 and a 98 μm long wires, respectively.

Mani et al [95M2] (page 245) investigated the two–terminal MR of parallel GaAs wires (Fig. 242). The SdH minima saturated to a temperature–independent behaviour in the vicinity of $\nu = 1$ and $\nu = 2$ at low T. At larger temperatures, $1.5\,\mathrm{K} \leq T \leq 5\,\mathrm{K}$, a $\nu = 1$ resistance minimum revealed localization and activated transport.

Gershenson et al [97G2] reported observation of a crossover from weak to strong localization in five parallel 40 μm long GaAs wires ((A) $w_{\mathrm{eff}} = 0.1\,\mu$m; (B) $w_{\mathrm{eff}} = 0.2\,\mu$m; $l = 20\,$nm) defined by EBL and ion etching. The temperature dependence of the resistance of sample A was consistent with the theory of quantum corrections due to weak localization and electron–electron interaction effects at high enough T. At low T, the dependence of R on T became exponential and was fitted with an activation law (Fig. 243). Below $T \approx 0.1\,$K, the increase of $R(T)$ saturated. The MR of the samples was negative over the whole temperature range. The activation energy decreased by a factor of ≈ 2 in strong fields. AF were observed whose amplitude increased with decreasing temperature. The phase coherence length was estimated from fits to the MR data, yielding $l_\varphi = 0.2 \pm 0.05\,\mu$m at 3 K and $0.05 \pm 0.01\,\mu$m at 30 K. At the crossover from weak to strong localization, l_φ became comparable to the localization length. Features of the MR in the regime of strong localization were in accordance with a doubling of the localization length in quasi 1D conductors in a strong magnetic field. Finally, Gershenson et al examined the magnetic–field dependence of the activation energy.

Khavin et al [98K4] (page 231) studied arrays of GaAs wires. In the temperature dependence of the resistance, a crossover from WL to SL was observed when T decreased below T_0.

Khavin et al [98K5] studied the resistance of arrays of GaAs wires fabricated by EBL and deep ion etching ($w_{\mathrm{eff}} = 0.05\,\mu$m, $L = 40\,\mu$m, 5 wires or $L = 500\,\mu$m, 470 wires; distance between the wires 1 μm). For several samples they repeated the measurements after deposition of a top–gate electrode. The number of transverse channels in the wires was $\approx 7 - 30$, $k_{\mathrm{F}} l = 6 - 40$. At high temperatures, the resistance increased slowly with decreasing T in accordance with WL theory, while it showed an activation–type behaviour at low T. This crossover from the WL to the SL regime occurred for $R \approx h/e^2$ and l_φ $2 - 3$ times smaller than the localization length ξ. On the SL side of the crossover the resistance was fitted by $R(T) = R_0 e^{T_0/T}$. For samples with the same diffusion constant, T_0 varied proportional to w^{-2}, $k_{\mathrm{B}} T_0$ was close to the level spacing Δ_ξ. With increasing carrier concentration, the activation energy decreased and ξ increased, while the

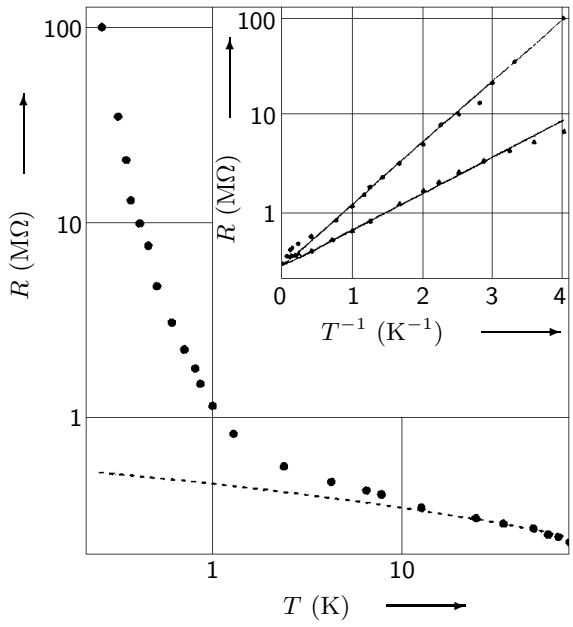

Fig. 243: Temperature dependence of the resistance in sample A at zero magnetic field [97G2]. The dashed curve is the sum of the weak–localization and the electron–electron interaction corrections to the resistance of a 2D sample. Inset: Logarithm of resistance vs. $1/T$ for sample A at $B = 0$ (bottom, triangles) and at $B = 6.4\,\mathrm{kOe}$ (top, circles). The straight lines correspond to the dependences $R(B = 0) = 0.28\,\mathrm{M\Omega}\,\exp(1.47\,\mathrm{K}/T)$ and $R(B = 6.4\,\mathrm{kOe}) = 0.28\,\mathrm{M\Omega}\,\exp(0.86\,\mathrm{K}/T)$.

product $T_0\xi$ was independent of gate voltage. The non–linear I–V characteristics was measured at different temperatures. For $V < 5\,\mathrm{mV}$, R was strongly temperature dependent, corresponding to the SL regime. In the WL regime for $V > 5\,\mathrm{mV}$, all $R(V,T)$ fell onto a single curve. Khavin et al estimated the distance between the critical hops L_c from fits of $R(V,T)$ in the SL regime. With decreasing T, L_c increased and exceeded ξ by more than an order of magnitude at $T/T_0 \gg 1$, but was always at least a factor ≈ 50 smaller than the wire length. For fixed T_0/T, L_c was proportional to ξ for different V_g. The temperature dependence of L_c contradicted predictions based on the VRH theory. The MR in the WL and the SL regime was negative and strongly anisotropic. The crossover shifted to lower temperatures in weak magnetic fields. The factor R_0 was independent of magnetic field, only the activation energy changed and thus ξ. The localization length doubled at a characteristic field due to breaking of the time–reversal symmetry. The density of states at the Fermi level increased by $\approx 40\%$ after deposition of the gate electrode, further T_0 decreased and L_c increased. The authors attributed this effect to screening of the long–range Coulomb interaction by the metal film.

8.9 References for Section 8

[73H] Harper, P.G., Hodby, J.W., Stradling, R.A.: Rep. Prog. Phys. **36** (1973) 1.

[82S1] Skocpol, W.J., Jackel, L.D., Hu, E.L., Howard, R.E., Fetter, L.A.: Phys. Rev. Lett. **49** (1982) 951.

[83S] Skocpol, W.J., Jackel, L.D., Howard, R.E., Hu, E.L., Fetter, L.A.: Physica **117B & 118B** (1983) 667.

[86P1] Pohlmann, H., Wassermeier, M., Kotthaus, J.P.: Superlatt. Microstruct. **2** (1986) 293.

[86W4] Warren, A.C., Antoniadis, D.A., Smith, H.I.: Phys. Rev. Lett. **56** (1986) 1858.

[87G2] Grassie, A.D.C., Hutchings, K.M., Lakrimi, M., Foxon, C.T., Harris, J.J.: Phys. Rev. B **36** (1987) 4551.

[88A] Alsmeier, J., Sikorski, Ch., Merkt, U.: Phys. Rev. B **37** (1988) 4314.

[88B1] Brinkop, F., Hansen, W., Kotthaus, J.P., Ploog, K.: Phys. Rev. B **37** (1988) 6547.

[88D] Demel, T., Heitmann, D., Grambow, P., Ploog, K.: Appl. Phys. Lett. **53** (1988) 2176.

[88P] Potts, A., Hasko, D.G., Cleaver, J.R.A., Ahmed, H.: Appl. Phys. Lett. **52** (1988) 834.

[89D2] Demel, T., Heitmann, D., Grambow, P., Ploog, K.: Superlatt. Microstruct. **5** (1989) 287.

[89I] Ismail, K., Antoniadis, D.A., Smith, H.I.: Appl. Phys. Lett. **54** (1989) 1130.

[89M5] Merkt, U.: Superlatt. Microstruct. **6** (1989) 341.

[89T6] Takagaki, Y., Ishibashi, K., Ishida, S., Takaoka, S., Gamo, K., Murase, K., Namba, S.: Jpn. J. Appl. Phys. **28** (1989) 645.

[89Y] Yamada, S., Asai, H., Fukai, Y.K., Fukui, T.: Phys. Rev. B **39** (1989) 11199.

[90G3] Gao, J.R., de Graaf, C., Caro, J., Radelaar, S., Offenberg, M., Lauer, V., Singleton, J., Janssen, T.J.B.M., Perenboom, J.A.A.J.: Phys. Rev. B **41** (1990) 12315.

[90H] Hirler, F., Smoliner, J., Gornik, E., Weimann, G., Schlapp, W.: Appl. Phys. Lett. **57** (1990) 261.

[90K3] Kern, K., Demel, T., Heitmann, D., Grambow, P., Ploog, K., Razeghi, M.: Surf. Sci. **229** (1990) 256.

[90P2] Potts, A., Hasko, D.G., Cleaver, J.R.A., Smith, C.G., Ahmed, H., Kelly, M.J., Frost, J.E.F., Jones, G.A.C., Peacock, D.C., Ritchie, D.A.: J. Phys.: Condens. Matter **2** (1990) 1807.

[90P3] Potts, A., Kelly, M.J., Smith, C.G., Hasko, D.G., Cleaver, J.R.A., Ahmed, H., Peacock, D.C., Ritchie, D.A., Frost, J.E.F., Jones, G.A.C.: J. Phys.: Condens. Matter **2** (1990) 1817.

[90S] Smith, C.G., Pepper, M., Newbury, R., Ahmed, H., Hasko, D.G., Peacock, D.C., Frost, J.E.F., Ritchie, D.A., Jones, G.A.C., Hill, G.: J. Phys.: Condens. Matter **2** (1990) 3405.

[90T5] Takagaki, Y., Gamo, K., Namba, S., Ishida, S., Takaoka, S., Murase, K.: J. Appl. Phys. **67** (1990) 340.

[91D] Demel, T., Heitmann, D., Grambow, P., Ploog, K.: Superlatt. Microstruct. **9** (1991) 285.

[91I2] Ismail, K., Washburn, S., Lee, K.Y.: Appl. Phys. Lett. **59** (1991) 1998.

[91L1] Lee, K.Y., Kern, D.P., Ismail, K., Washburny, S.: J. Vac. Sci. Technol. B **9** (1991) 2834.

[91N] Nakata, S., Hirayama, Y., Tarucha, S., Horikoshi, Y.: J. Appl. Phys. **69** (1991) 3633.

[91P2] Potts, A., Kelly, M.J., Hasko, D.G., Smith, C.G., Cleaver, J.R.A., Ahmed, H., Peacock, D.C., Frost, J.E.F., Ritchie, D.A., Jones, G.A.C., Singleton, J., Janssen, T.J.B.M.: Superlatt. Microstruct. **9** (1991) 315.

[92B4] Bagwell, P.F., Park, S.L., Yen, A., Antoniadis, D.A., Smith, H.I., Orlando, T.P., Kastner, M.A.: Phys. Rev. B **45** (1992) 9214.

[92K1] Kurdak, C., Chang, A.M., Chin, A., Chang, T.Y.: Phys. Rev. B **46** (1992) 6846.

[92K4] Kelly, M.J., Potts, A., Hamilton, A., Tewordt, M., Pepper, M., Law, V.J., Frost, J.E.F., Ritchie, D.A., Jones, G.A.C., Hasko, D.G., Ahmed, H.: Phys. Scr. T **45** (1992) 200.

[92M2] Mani, R.G., von Klitzing, K.: Phys. Rev. B **46** (1992) 9877.

[92M3] Mori, N., Momose, H., Hamaguchi, C.: Phys. Rev. B **45** (1992) 4536.

[92P2] Potts, A., Kelly, M.J., Hasko, D.G., Cleaver, J.R.A., Ahmed, H., Ritchie, D.A., Frost, J.E.F., Jones, G.A.C.: Semicond. Sci. Technol. **7** (1992) B231.

[93B4] Berthold, G., Smoliner, J., Wirner, C., Gornik, E., Böhm, G., Weimann, G., Hauser, M., Hamaguchi, C., Mori, N., Momose, H.: Semicond. Sci. Technol. **8** (1993) 735.

[93C1] Carpi, E.L., van Hove, M.: Superlatt. Microstruct. **14** (1993) 53.

[93G2] Gusev, G.M., Basmaji, P., Kvon, Z.D., Litvin, L.V., Nastaushev, Yu.V., Toropov, A.I.: Sol. St. Commun. **85** (1993) 317.

[93H2] Hasko, D.G., Cleaver, J.R.A., Ahmed, H., Smith, C.G., Dixon, J.E.: Appl. Phys. Lett. **62** (1993) 2533.

[93M3] Mani, R.G., von Klitzing, K., Ploog, K.: Phys. Rev. B **48** (1993) 4571.

[93M4] Motohisa, J., Sakaki, H.: Appl. Phys. Lett. **63** (1993) 1786.

[94H3] Hauser, M., Gornik, E., Wirner, C., Baur, M., Böhm, G., Weimann, G.: Semicond. Sci. Technol. **9** (1994) 951.

[94H4] Holzmann, M., Többen, D., Abstreiter, G., Schäffler, F.: J. Appl. Phys. **76** (1994) 3917.

[94M5] Mani, R.G., von Klitzing, K., Vasiliadou, E., Grambow, P., Ploog, K.: Surf. Sci. **305** (1994) 654.

[95H4] Holzmann, M., Többen, D., Abstreiter, G., Wendel, M., Lorenz, H., Kotthaus, J.P., Schäffler, F.: Appl. Phys. Lett. **66** (1995) 833.

[95M2] Mani, R.G., von Klitzing, K., Ploog, K.: Phys. Rev. B **51** (1995) 2584.

[95R1] Reulet, B., Bouchiat, H., Mailly, D.: Europhys. Lett. **31** (1995) 305.

[96H3] Holzmann, M., Többen, D., Baumgartner, P., Abstreiter, G., Kriele, A., Lorenz, H., Schäffler, F.: Surf. Sci. **361/362** (1996) 673.

[96P1] Ploner, G., Smoliner, J., Strasser, G., Gornik, E.: Physica B **227** (1996) 24.

[96S1] Sasa, S., Sugihara, T., Tada, K., Izumiya, S., Yamamoto, Y., Inoue, M.: Physica B **227** (1996) 363.

[97G2] Gershenson, M.E., Khavin, Yu.B., Mikhalchuk, A.G., Bozler, H.M., Bogdanov, A.L.: Phys. Rev. Lett. **79** (1997) 725.

[97M] Maemoto, T., Yamamoto, H., Konami, M., Kajiuchi, A., Ikeda, T., Sasa, A., Inoue, M.: phys. stat. sol. b **204** (1997) 255.

[97P] Ploner, G., Smoliner, J., Strasser, G., Gornik, E.: Superlatt. Microstruct. **22** (1997) 249.

[98K3] Katine, J.A., Berry, M.J., Westervelt, R.M., Gossard, A.C.: Phys. Rev. B **57** (1998) 1698.

[98K4] Khavin, Yu.B., Gershenson, M.E., Bogdanov, A.L.: Phys. Rev. Lett. **81** (1998) 1066.

[98K5] Khavin, Yu.B., Gershenson, M.E., Bogdanov, A.L.: Phys. Rev. B **58** (1998) 8009.

[98L] Lefebvre, J., Beerens, J., Feng, Y., Wasilewski, Z., Beauvais, J., Lavallée, E.: J. Vac. Sci. Technol. B **16** (1998) 2915.

[98P2] Ploner, G., Smoliner, J., Strasser, G., Hauser, M., Gornik, E.: Phys. Rev. B **57** (1998) 3966.

[98T3] Tang, Y., Rich, D.H., Moy, A.M., Cheng, K.Y.: Appl. Phys. Lett. **72** (1998) 55.

[99F2] Friedland, K.J., Schönherr, H.P., Nötzel, R., Ploog, K.H.: Phys. Rev. Lett. **83** (1999) 156.